CHAPTER 1 INTRODUCTION

1.1 INTRODUCTION

As sources of the petroleum and natural gas are gradually depleting, renewable energy sources such as wind, biomass, photovoltaic and geothermal energy may become more important in the future (Borman, 1998). Access to modern energy system is absolutely necessary for development yet two billion people the world over currently go without it, live in poverty. The fundamental dilemma is that, despite energy being a vital ingredient for growth, sustainable development and for the vast majority of economic activities, its production and use, contribute to global warming. Therefore, the energy sector today is confronted with the greatest challenge of mitigating the rising demand for modern energy services, while at the same time, reduce emissions of greenhouse gases (André, 2007).

The annual solar radiation in Zambia is amongst the highest in the world. The radiation is fairly uniform across the country, varying in the range of 6,600-7,700 MJ/m^2 (5.27- 6.09kWh/m^2), (UNEP, 2005). With this abundant solar resource, it is expected that the utilisation of solar energy in engineering especially; solar water heaters, lighting and refrigeration of medicines at rural health centers will become widespread in the near future. Therefore, the focus of this thesis is on the estimation of solar radiation for locations in Zambia especially, where this resource is not measured.

1.2 WORLD ENERGY SENERIO

The world is increasingly aware that fundamental changes will be necessary to meet the growing demand for energy (Jerome, 2008). A number of energy scenarios are suggested by several organizations. These organizations include the International Energy Agency (IEA), the United States Energy Information Administration (EIA) and the World Energy Council (WEC). All these foresee substantial global energy demand increase by 2050. With the current trend, there will be dramatic change in the way energy is produced and consumed, global energy consumption will double by 2050 and CO_2 emissions will continue to rise and reach to two-and-a- half times the current levels.

According to the IEA report (2009), global energy scenarios, clearly demonstrate how to achieve a clean, clever and competitive energy future by 2050. IEA reports three sets of scenarios: Baseline, Accelerated Technology (ACT) Map and the BLUE Map.

The Baseline Scenario (business as usual) simply looks at the future as a continuation of the past and present. Under this scenario energy consumption will double by 2050 and CO_2 emissions will continue to rise and reach to two-a-half times the current levels. This is after taking in account the efficiency gains and the technological progress that are expected under existing policies.

According to the ACT Scenario, energy consumption will be about 77% of the baseline scenario and energy related CO_2 emissions will reduce to their 2005 levels by 2050. This scenario also indicates that by 2050, the energy efficiency measures could reduce electricity demand by a third below the baseline levels.

With the BLUE Map Scenario, energy consumption will be about 67% of the baseline scenario and the CO_2 emissions will be 50% lower than the 2005 levels. This scenario explores the least cost solutions to achieve this goal and limit the risks of severe climate change. To meet the objectives of the BLUE scenario, we must develop and implement far-reaching new policies to substantially "decarbonize" power generation. Both ACT and BLUE Scenarios require extensive use of renewable energy resources which would provide 35% and 46% of the total global power generation requirements.

The major driving forces of the world energy demand and supply could be clustered into nine groups as follows: energy consumption growth rate; demographic changes; economic growth rate; investment requirements; CO_2 emissions; technological development and innovations; global energy intensity; oil price and development of alternative energy sources (Nezhad, 2009).

Table 1.1 shows the total global energy consumption in 2005 and the three scenarios, while Figure 1.1 shows the energy consumption by building, transport and industry sectors in 2005.

Table 1.1 World Total Energy Consumption in 2005 and the three Scenarios for 2005 (Mtoe/yr)

	2005	Baseline	ACT Map	BLUE Map
Total end-use	7,748	15,683	12,076	10,553

Source: 2009 World Energy scenarios to 2050: Issues and Options.

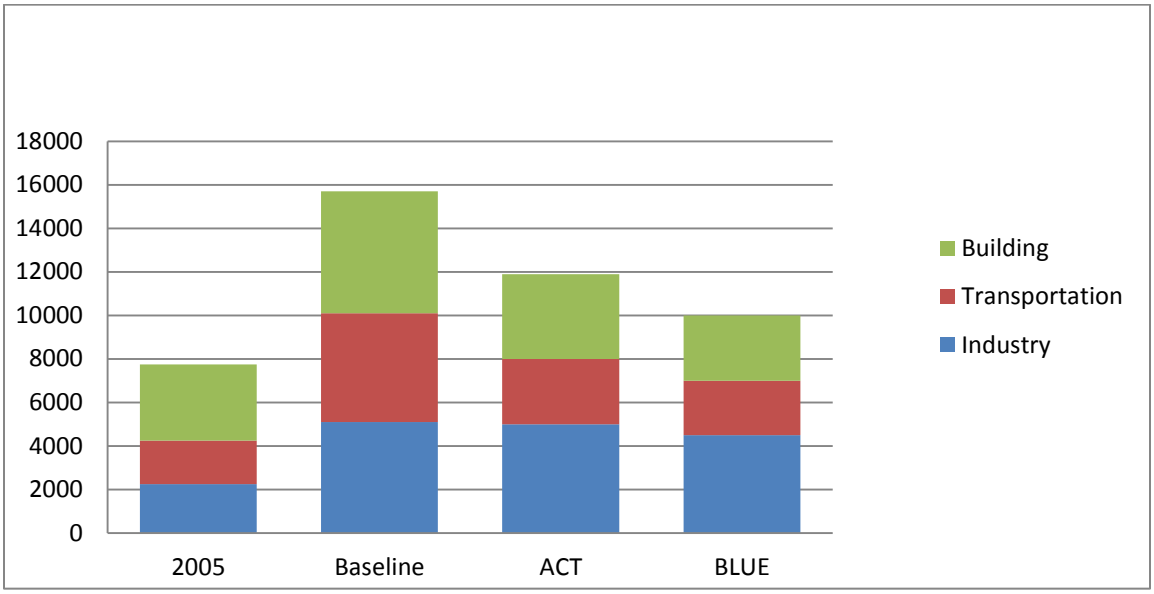

Figure 1.1 Energy consumption by sector in 2005 and the three scenarios (Mtoe/yr)

Source: 2009 World Energy scenarios to 2050: Issues and Options.

The extent of global fuel reserves is subject to debate. Natural gas and crude oil reserves are more limited than coal. The term reserves means estimated amounts in the ground that geological data demonstrate with reasonable certainty to be recoverable in future years under existing economic and operating conditions. Hence, this includes undiscovered reserves. The world production rates of natural gas, crude oil and coal are shown in Table 1.2 along with the time to deplete the fuel reserves at the current production rates. Natural gas will be depleted in 123 years, crude oil in 67 years and coal in 230 years at the current production rates. These estimates of the time to consume the fossil fuels of the world are problematic because new exploration may expand or reduce the reserve figures, while increasing consumption driven by rising population and unmet human needs will decrease the depletion time (Borman et al., 1998).

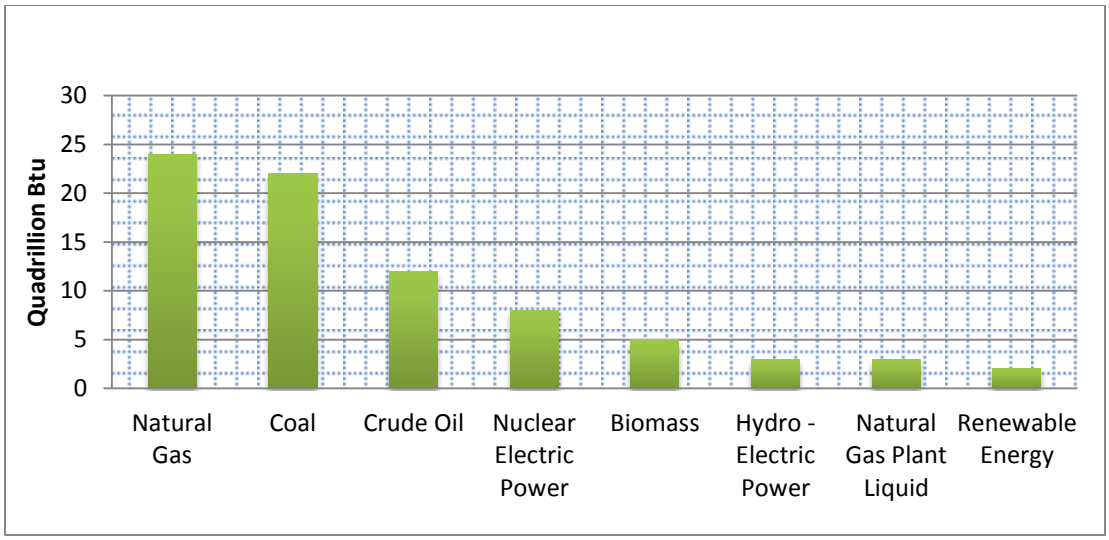

Figure 1.2 Primary Energy Production by Source

Table 1.2 World Fossil Fuel Production Rate [Energy Info. Admin. 1994]

Fuel	**1993 Production**	**Supply at 1993 Production Rate**
Natural Gas	75 trillion ft3	123 years
Crude Oil	23 billion barrels	67 years
Coal	4.1 billion tons	230 years

Source: (Borman et al.,1998)

1.3 ENERGY SCENARIO IN ZAMBIA

By far, the largest source of energy in Zambia is traditional biomass such as wood and charcoal. However, Zambia has abundant hydroelectric resources and meets most of its energy needs from the generation of hydroelectric power stations. About 99.9% of electricity produced comes from hydro. Zambia imports all of its fossil fuels, apart from a small amount of coal (Recipes, 2006).

Zambia Electricity Supply Corporation (ZESCO) is a parastatal company mandated to generate, transmit and distribute power in Zambia. Table 1.3 shows the major hydropower plants while Table 1.4 shows the small hydropower plants with their generating capacities for ZESCO. In 2004/05, ZESCO generated 8,816GWh in total, which almost matches the electricity consumption in Zambia.

Table 1.3 Three Major Hydropower Plants in Zambia

Name of Hydro Power Plant		Kariba North Bank	Kafue Gorge	Victoria Falls
Number of Units		4	9	14
Original Installed Capacity		600MW	900MW	108MW
Available Capacity (Sep. 2006)		660MW	630MW	108MW
Expected Capacity after Rehabilitation		720MW	990MW	108MW (Completed)
Electricity Generation	FY2001/02	2,886GWh	5,570GWh	602GWh
	FY2002/03	2,790GWh	4,806GWh	448GWh
	FY2003/03	3,158GWh	4,668GWh	354GWh
	FY2004/05	3,644GWh	4,073GWh	269GWh
	FY2005/06	3,661GWh	4,619GWh	537GWh

Source: ZESCO 2005 Annual Report

Table 1.4 Small Hydro Power Plants

Name		Lusiwasi	Musonda	Chishimba	Lunzua
Province		Central	Luapula	Northern	Northern
Installed Capacity		12MW	5MW	6MW	0.75MW
Available Capacity		12MW	5MW	6MW	0.75MW
Number of Units		3MW x 4	1MW x 5	1.2MW x 4 0.3MW X4	0.25MW x 3
Electricity Generation	FY2001/02	9.8GWh	17.7GWh	5.5GWh	2.0GWh
	FY2002/03	15.7GWh	15.8GWh	7.0GWh	2.7GWh
	FY2003/03	17.7GWh	15.4GWh	16.6GWh	1.1GWh
	FY2004/05	13.7GWh	17.2GWh	16.9GWh	1.7GWh
	FY2005/06	3.7GWh	17.0GWh	16.3GWh	1.7GWh

Source: ZESCO 2005 Annual Report

1.3.1 Electricity Generating Facilities for Private Companies

(a) Lunsemfwa Hydropower Company

Lunsemfwa Hydropower Company (LHPC) is an independent power producer located in the Central Province of Zambia. LHPC has two Hydropower Stations namely, Lunsemfwa Hydropower Plant in Mkushi District (18MW) and Mulungushi Hydropower Plant in Lunsemfwa District (20MW).

(b) Copperbelt Energy Corporation

Copperbelt Energy Corporation (CEC) procures electricity supply mostly from ZESCO for its own customers. It transmits and distributes electricity to most mining companies on the

Copperbelt. CEC operates 80MW emergency gas thermal turbines as well as transmission and distribution networks of about 808 km overhead lines and 36 high voltage substations.

(c) Konkola Copper Mines

Konkola Copper Mines (KCM) has a 20MW Nkana Gas Thermal Power Plant in Kitwe on the Copperbelt and is the leading copper mining company in Zambia. KCM usually purchases electricity from CEC and the 20 MW Gas thermal Power Plant is maintained as standby emergency power.

(d) Off-grid Power Generation in Zambia

Off-grid power generation plays an important role in supplying electricity to the areas which are far from the national grid. The power supply in such cases is through isolated small distribution networks, so-called "micro-grid", with small diesel or hydropower plants. However, in some areas where even an isolated grid is far from being economically viable, installing solar systems on site can be the only way of electricity supply. Table 1.6 shows the existing Micro-Hydro Power Plants in Zambia that supply electricity through an isolated micro-grid.

(e) Diesel Power Generation

ZESCO has diesel power plants in some remote areas, and about half of them are located in North-Western Province. Table 1.5, shows ZESCO diesel power plants while Table 1.6 gives the existing micro-hydro power plant.

Table 1.5 ZESCO Diesel Power Plants.

Name	Kabompo		Zambezi	Chavuma	Mufumbwe	Mwinilunga
Province	North-Western		North-Western	North-Western	North-Western	North-Western
Capacity	1,560kW		800kW	690kW	320kW	1,430kW
Generation Y2005/06)	2.7GWh		2.5GWh	N.A.	0.97GWh	2.4GWh
Name	Luangwa	Lukulu	Kaputa	Chama	Kaoma	Kasempa
Province	Lusaka	Western	Northern	Eastern	Western	North-Western
Capacity	732kW	512kW	486kW	263kW	2,620kW	530kW
Generation (FY2005/06)	1.1GWh	0.83GWh	1.0GWh	0.5GWh	0.27GWh	N.A.

Source: ZESCO 2005 Annual Report

Table 1.6 Existing Micro-Hydro Power Plant

Name	Nyango'mbe	Luakela	Mutanda	Lwawu
Installed Capacity	77kW	35kW	2.5kW	50kW

Source: ZESCO 2005 Annual Report

1.4 RENEWABLE ENERGY IN ZAMBIA

Zambia has potential of renewable energy such as biomass, geothermal, and wind-power sources, and the Government of the Republic of Zambia has been keen in expanding the use of these resources.

Table 1.7 Availability and Potential for Utilization of Renewable of Energy Resources and Technologies in Zambia

Renewable Energy	Opportunities/Use	Resource Availability	Potential Energy Output
PV	Thermal (water heating), Electricity (water pumping, lighting, refrigeration)	6-8 sunshine hours	5.5 kWh/m^2/day (modest potential especially for limited irrigation)
Wind	Electricity Mechanical (water pumping)	Average 3m/s	Good potential, especially for irrigation
Micro-hydro	Small grids for electricity supply	Reasonably extensive	Requires elaboration and quantification
Biomass (combustion and Gasification)	Electricity generation	Agro wastes Forest wastes Sawmill wastes	Requires elaboration and quantification
Biomass (biomethanation)	Electricity generation Heating and cooking	Animal waste Agro- and industrial waste Waste water	Potential requires elaboration
Biomass (extraction, processing for transport)	Ethanol for blending with gasoline to replace lead as octane enhancer Biodiesel for stationary engines	Sugarcane Sweet sorghum Jatropha	15,000 ha to meet current demand
Biomass (for household energy)	Improved charcoal production Improved biomass stove	Sawmill wastes and indigenous trees from sustainable forest management	Reasonably extensive

Source: National Energy Policy (MEWD), 2006.

There are two major geothermal energy developments currently under consideration in Zambia. The first one is the Kapishya Geothermal Project, located in Nsumbu on the shores of Lake Tanganyika. The plant has fifteen shallow exploratory and production wells and submersible

pumps have been installed in four of them. Two Organic Rankine Cycle (ORC) turbo-generators, with a nominal capacity of 200 kW, were installed.

The second project involves the development of a health resort and the potential construction of a geothermal power plant providing cheap electric power to the local community at Chinyunyu Hot Springs, located 50 kilometres east of Lusaka on Great East Road. This project was undertaken by the Japanese International Cooperation Agency (JICA), in conjunction with the Zambian Geological Survey (Recipes, 2006).

1.5 SOLAR ENERGY IN ZAMBIA

The contribution of solar energy to the electrification of Zambia is quite minor. Figure 1.3 shows the solar radiation map of Zambia. There is not much discrepancy among regions in annual solar radiation, which is recorded relatively high and stable between 6,600 and 7,700MJ/m^2 p.a., which means that Zambia has potential for the solar energy all over the country.

Zambia's national land area is 752,600 km^2, and when assumed that 0.001% of the land is used for the solar generation, about 1,200GWh can be potentially generated. Assuming operation rate of 80%, this is equivalent to 170MW scale power plant. Therefore, the utilization of Zambia's high potential for solar generation is one of effective measures for rural electrification ((JICA), 2007).

Potential Electricity Generation from Solar Power (kWh/year) = Average Solar Radiation (kWh/ m^2/day) × Land Area (km^2) ×365 (day/year) × 10^6 Eqn.1.1

- Average Solar Radiation (kWh/m^2/day) : 4.35
- Land Area : 752,610km^2
- Land Utilization : 0.1%
- Conversion Efficiency : 10%
- Unit Measurement : 1MJ/m^2 =23.89cal/cm^2
  =238.9kcal/m^2 =0.2778kWh/m^2

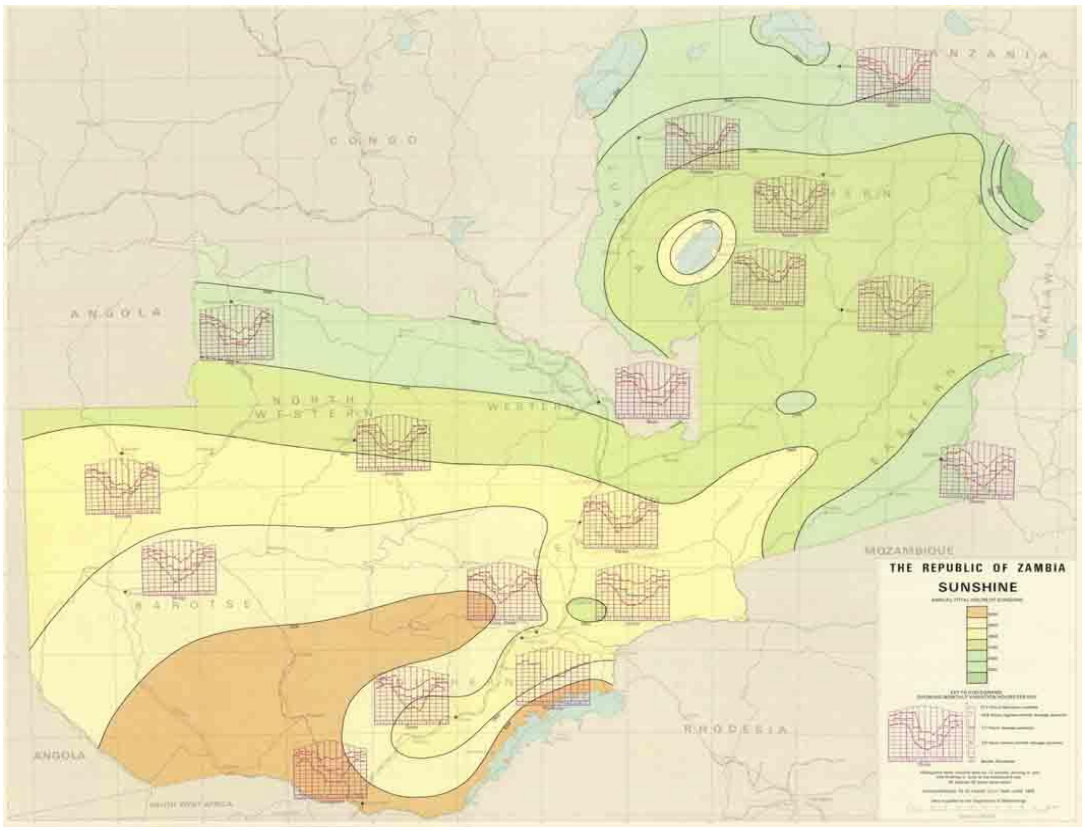

Figure 1.3 Solar Radiation Map of Zambia. Source: Department of Meteorology

1.6 A BRIEF REVIEW OF SOLAR RADIATION MODELLING

Solar radiation is the major and direct energy input into the terrestrial ecosystem. It is the primary driving force of all physical, biological and industrial systems. The Sun gives a natural influence on climate and the earth's atmosphere (Colorado, 2003). In the absence of the Sun, the earth would have been like a frozen rock stranded in the universe. The energy from the Sun warms the earth making life possible. This energy cleanses our water, generates clouds, produces plants, keep humans and animals warm, drives ocean currents and thunderstorms. In spite of the Sun's importance, scientists only began to study it with high precision in recent decades. In fact, prior to 1979, Earth Scientists and Astronomers were unable to accurately determine the total amount of energy from the sun that reaches the earth's outermost atmosphere. The variable absorption of sunlight by aerosols and clouds hampered researchers to accurately measure solar radiation just before it strikes the earth's atmosphere (Weier, 2003).

The Solar Radiation and Climate Experiment (SORCE) a NASA-sponsored satellite mission, measures the sun's output using the state-of-the-art radiometers, photodiodes, spectrometers, and

photomultiplier tubes mounted on a satellite observatory. The SORCE is a free-flying, Earth-orbiting satellite which carries four instruments to measure the solar radiation incident at the top of the earth's atmosphere. These spectral measurements identify the solar radiation of the Sun by characterizing the Sun's energy over the full wide spectral range from ultraviolet to infrared. Data measured using SORCE experiment is used to model the sun's output in order to explain and predict the effect of the Sun's radiation on climate and the earth's atmosphere (Weier, 2003).

Determining the solar radiation and its interaction with the atmosphere and the earth's surface is important, since solar radiation accounts for almost all of the energy available on earth. There are two different methods through which data for solar radiation energy can be obtained. The first method, which is more accurate, is the direct measurement of solar radiation components using Pyranometers and Pyrheliometers. The second approach relies on empirical-analytical relationships that can predict the solar radiation components as a function of latitude, time, altitude, zenith angle, hours of measured sunshine, clear sky conditions, etc. The latter can be used in locations with similar meteorological and geographical characteristics where measured data on solar radiation energy is not available due to limited coverage of radiation measuring networks. Unfortunately, for many developing countries, Zambia inclusive solar radiation measurements are not easily available due to cost, maintenance and calibration requirements of measuring equipment (El-Sebaii et al., 2005).

1.7 PROBLEM STATEMENT

A pervasive dearth of solar radiation knowledge exists in Africa, with Zambia being a typical case (Nasitwitwi et al., 2000). However, the understanding of the amount of solar radiation at various geographic locations is desirable for applications such as solar energy utilization, environmental assessment, civil engineering, forestry, meteorology, agriculture and ecological research (Rich, 2006).

Although solar radiation is measured, in Zambia, by the Meteorological Department in the Ministry of Transport and Communication, only few isolated locations namely: Mansa, Kasama, Mfuwe, Lusaka, Ndola, Livingstone and Mongu are covered. In fact, the baseline trend is that at some of these locations, measuring of solar radiation has been discontinued partially due to the following reasons:

i. Malfunctioning of equipment;
ii. Incompleteness of equipment; and
iii. Lack of calibration of equipment.

Additionally, for most geographical areas in Zambia, insolation data is not available probably due to the **cost**, **maintenance** and **calibration** requirements of measuring equipment.

However, in order to effectively and efficiently utilize this abundant solar energy resource that the country is endowed with, the starting point is to create insolation database for various geographic locations. The best solar radiation database is the long term measured data at sites of the intended solar system. However, due to the limited coverage of radiation measuring networks dictates, there is need for developing solar radiation models (Chow, 2001). It is for this reason that the following research questions were to be answered.

1.8 OBJECTIVES OF THE RESEARCH

The general objective of the study was to develop empirical/ analytical models which could be used to predict the monthly mean direct, diffuse and global solar radiations on a horizontal surface for selected locations in Zambia where no measured solar radiation data is available but model parameters could be obtained locally.

The specific objectives of this research were:

1. To collect and analyze Geographical, Geometrical, Astronomical and Meteorological (GGAM) parameters data, ground based and satellite-derived solar radiation data sets at selected sites in Zambia.
2. To use the analyzed data to develop general mathematical models for estimating monthly mean global solar radiation intensities.
3. To use the developed mathematical models to estimate solar radiation model for Zambia where no measured data is available but model parameters obtainable locally.
4. To test the developed models for accuracy.

1.8.1 Research Questions to be answered

i. How can global solar radiations for locations in Zambia where no measured data is available be estimated?
ii. How do ground and Satellite-derived solar radiation data sets in Zambia compare?

1.8.2 Benefits of the Research

The benefits of this research shall be to:

- develop models that will be used to generate sufficiently accurate solar radiation database for Zambia where there is limited coverage of radiation measuring networks.
- develop solar radiation map for Zambia.
- establish a scholarly method for developing models to estimate solar radiation for any site

1.9 JUSTIFICATION OF THE RESEARCH

Although Zambia has abundant hydropower, which is estimated at 6000 MW potential (currently installed capacity is about 1788 MW), only 50% of the urban population has access to electricity, and only 2-3% of the rural population has been connected to the national power grid. The large land span and sparse population in Zambia have made it difficult to extend the national power grid to far -flung rural areas and is very expensive and is cross-subsidized by a uniform electricity tariff. The baseline trend is that supply of power in many remote rural areas is predominately serviced by diesel engine powered generators, facing high imported diesel fuel cost with consequent environmental impacts. Thus, Zambia has an ideal opportunity to promote the use of abundant renewable energy resources - biomass, solar, and mini-hydro, that are indigenously available to facilitate the rural electrification and promote linked productive use activities. A number of barriers including financial, institutional, technical, information and human resource constrain the increased use of renewable energy sources in the rural areas of Zambia (UNEP, 2005).

The capability of a power system to transmit electricity has limitations depending on the capacity of equipment and system condition. If, with the implementation of an electrification project, the maximum power load at local level exceeds the system capability of that area, then reinforcement of transmission system is inevitable and its cost should be added to the cost of the

electrification project. This is why the analysis of the capability of local network systems, i.e. the capability of each substation, needs to be carried out for an electrification study (JICA, 2007)

Also with the increased mining and construction activities taking place in the country, the demand for power has increased resulting in undesired power load shedding. This inadequate power and high tariff have resulted in most people using the traditionally and inefficiently produced charcoal from forest resources which is a low energy content source, which pollutes the environment.

According to the draft Rural Electrification Master Plan Study in Zambia (JICA,2007), as shown Table 1.8 below shows that the electrification rate for households is 20.3% in Zambia as of 2004 while from the "Living Conditions Monitoring Survey 2004" conducted by the Central Statistics Office, the majority of Zambians (84.9% in rural area and 54.2% in whole country) use collected firewood and only 1.7 % of households in rural area use electricity as their main source of energy for cooking, Table 1.8 (JICA, 2007).

Table 1.8 Percentage Distribution of Households by Main Source of Energy for Lighting

		Kerosene / Paraffin	Electricity	Candle	Diesel	Open Fire	Others	None	Total	Total Nr. of Households	% of Total Population
Zambia	**Total**	**45.7%**	**20.3%**	**18.1%**	**7.4%**	**6.1%**	**1.4%**	**0.9%**	**100.0%**	**2,110,640**	**100.0%**
Total	Rural	62.3%	3.1%	9.7%	11.6%	9.9%	2.0%	1.5%	100.0%	1,288,065	61.0%
	Urban	19.5%	47.6%	31.5%	0.9%	0.2%	0.3%	0.1%	100.0%	822,575	39.0%
Provinces	Central	53.8%	12.4%	16.8%	13.3%	1.9%	1.3%	0.6%	100.0%	207,197	9.8%
	Copperbelt	29.2%	44.3%	20.7%	4.2%	0.9%	0.6%	0.1%	100.0%	311,712	14.8%
	Eastern	61.3%	8.2%	13.3%	8.7%	5.4%	1.6%	1.5%	100.0%	290,224	13.8%
	Luapula	80.9%	4.4%	4.1%	0.4%	9.5%	0.4%	0.4%	100.0%	171,659	8.1%
	Lusaka	12.6%	46.1%	39.8%	0.5%	0.2%	0.6%	0.2%	100.0%	309,949	14.7%
	Northern	70.4%	9.6%	5.3%	5.3%	7.4%	1.2%	0.9%	100.0%	275,266	13.0%
	North-Western	36.7%	11.1%	14.3%	22.0%	13.7%	1.4%	0.8%	100.0%	125,814	6.0%
	Southern	41.4%	15.7%	19.5%	15.5%	5.3%	1.1%	1.4%	100.0%	252,423	12.0%
	Western	39.2%	4.2%	19.3%	4.5%	23.9%	5.5%	3.4%	100.0%	166,219	7.9%

Source: Living Conditions Monitoring Survey Report 2004 (Central Statistical Office, December 2006)

Table 1.9 Percentage Distribution of Households by Main Source of Energy for Cooking

		Collected Firewood	Purchased Firewood	Own Produced Charcoal	Purchased Charcoal	Coal	Kerosene / Paraffin / Gas	Electricity	Others	Total
Zambia Total	**Total**	**54.2%**	**1.9%**	**3.5%**	**23.8%**	**0.0%**	**0.2%**	**16.2%**	**0.1%**	**100.0%**
	Rural	84.9%	1.7%	4.7%	6.6%	0.0%	0.2%	1.7%	0.2%	100.0%
	Urban	5.6%	2.2%	1.5%	51.1%	0.0%	0.2%	39.3%	0.0%	100.0%
Provinces	Central	68.2%	1.8%	1.0%	19.4%	0.0%	0.2%	9.3%	0.1%	100.0%
	Copperbelt	16.0%	1.4%	3.6%	41.7%	—	0.2%	37.0%	0.1%	100.0%
	Eastern	76.9%	2.7%	0.5%	14.6%	—	0.3%	4.9%	0.3%	100.0%
	Luapula	45.8%	3.1%	24.0%	24.4%	—	0.1%	2.4%	0.2%	100.0%
	Lusaka	10.7%	0.8%	0.8%	47.3%	0.0%	0.2%	40.2%	0.0%	100.0%
	Northern	75.2%	1.0%	3.2%	14.0%	0.1%	0.2%	6.4%	0.0%	100.0%
	North-Western	71.7%	1.5%	2.3%	15.9%	0.1%	0.5%	7.7%	0.2%	100.0%
	Southern	71.1%	2.5%	0.7%	13.4%	0.1%	0.2%	12.0%	0.1%	100.0%
	Western	88.3%	3.8%	0.6%	3.6%	—	0.2%	3.2%	0.4%	100.0%

Source: Living Conditions Monitoring Survey Report 2004. (Central Statistical Office, December 2006)

The availability of solar radiation energy in Zambia is tremendous, though the technology to convert this energy into heat and electricity is yet to be fully established. Therefore, to control and use this enormous source of energy needs an understanding of the variations and parameters influencing the solar radiation energy available in a place, both quantitatively and qualitatively. The knowledge of the global solar radiation is of fundamental importance for all solar energy conversion system. The solar radiation data are not easily available for many countries. Many countries cannot afford the measuring equipment and techniques involved. Therefore, it is rather important to develop methods to estimate the solar radiation using whatever weather parameters are available (Safaripour et al., 2011). It is easier to measure temperature, humidity, cloud cover, sunshine durations, etc. and use these parameters in a solar radiation model than measuring the actual solar radiation of any location.

Previously, similar research looked at only estimating **global solar radiations** for Zambia; with, **only sunshine hours considered as** Angstrom model was used. However a number of factors affect solar radiation reaching the horizontal surface were considered to improve the accuracy and subsequently the database that could be generated (Jain et al., 1988).

Ground-based measurements and satellite-derived solar radiation data complement each other and are necessary to build a comprehensive solar radiation database. It is impractical to have a high density ground-based solar radiation monitoring network that would give anywhere near the coverage capability of a satellite-derived solar radiation database. (Vignola, 2006) Traditionally, solar radiation is measured using networks of meteorological stations. However, the costs for installation and subsequently, maintenance of meteorological networks are quite high and this makes national networks to comprise only of few stations. Therefore, the availability of solar radiation measurements has shown to be spatially inadequate for many applications. Mapping solar radiation by way of interpolation and/ or extrapolation of measurements is possible but usually leads to large errors, except for dense networks. (Journ´ee, 2010) Thus, there is need to compare satellite derived and ground measured solar radiation data in order to ascertain the accuracy and reliability.

1.10 METHODOLOGY OF THE RESEARCH

The general method involved the correlation of Geographical, Geometrical, Astronomical and Meteorological (GGAM) data with Solar Radiation reaching the Horizontal Surface in Zambia. Using regression analysis techniques a general mathematical model to predict the Solar Radiations was developed for Zambia. These GGAM parameters obtained locally were namely: the average daily ratio of sunshine duration $\left(\frac{n}{N}\right)$; the mean daily extraterrestrial solar radiation (H_o); the mean daily relative humidity (R_h); the mean daily maximum dew point temperature ($T_{dp,\,max}$); the sunshine duration; relative humidity; the mean daily atmospheric pressure (P); and the solar declination angle (sine δ) and the amount of cloud cover (C).

The measured data sets of solar radiation and GGAM parameters obtained from the Meteorological Department in Zambia for selected sites were used.

In this research, solar model developed would take the form of:

$$H = a + b\sin\delta + cH_o + d\,{}^{n}/_{N} + eR_h + fT_{max} + gT_{dp,max} + hP + C \quad \text{Eqn.1.2}$$

H_o is the monthly mean daily extraterrestrial solar radiation,

n/N is the monthly average daily ratio of sunshine duration,

R_h is the mean daily relative humidity,

T_{max} is the monthly mean daily maximum air temperature

$T_{dp,max}$ is the monthly mean daily maximum dew point temperature

P is the monthly mean daily atmospheric pressure

$Sin\delta$ is the sine of the solar declination angle

C is the monthly mean of the cloud cover,

H is the predicated monthly mean daily global solar radiations

The regression coefficients $a, b, c, d, e, f, g\ and\ h$ were determined with the help of an advanced computer program **MATLAB 2011b** software.

The coefficient of correlation (CC) and standard errors (SE) for each of the seven models were calculated and tested for accuracy. Finally, developed correlations were then combined to determine one for estimating global solar radiation for all locations in Zambia. Ground measured solar radiation data for the selected sites in Zambia was also compared with satellite derived one provided by web-based systems and databases to ascertain the accuracy and reliability for application in design.

1.11 BRIEF CHAPTERS OVERVIEW

In addition to this introductory Chapter 1, the thesis also includes Chapter 2, 3, 4 and 5. Chapter 2 reviews the literature in the field of solar radiation modelling. In Chapter 3, a detailed methodology is presented while Chapter 4 gives results analysis and discussion; and finally, Chapter 5 gives the conclusions.

1.12 CONCLUSION

This Chapter lays the foundations for the thesis. It introduced the research problem and research questions. Then the research was justified, methodology was described and the thesis outlined briefly. On these foundations, the thesis can now proceed with a detailed description of the research.

CHAPTER 2 SOLAR RADIATION MODELLING

2.1 INTRODUCTION

The entire process of solar radiation modeling is centered on the estimation of the model parameters from a given set of data (Sen, 2008). In order to understand the behavior of solar radiation modelling, two approaches can be used:

a. **Physical Modeling**: this looks at the physical processes in the atmosphere such as molecular gases, water vapour, aerosols, or clouds. Part of this radiation is backscattered to space, another part is absorbed and the rest falls into the earth's surface. This latter component interacts with the surface. Therefore, the diffuse radiation is composed of the radiation backscattered by the atmosphere before reaching the ground and the component reflected by the earth's surface. Finally, the radiation on the surface depends on the absorption and scattering processes in the atmosphere. The physical method is exclusively based on physical considerations, allowing the radiant energy exchanges take place within the earth-atmosphere system. This approach dictates models that account for the estimated solar irradiation at the ground in terms of certain number of physical parameters (water vapour content, dust, aerosols, clouds and cloud type, etc.).

b. **Statistical Solar Climatology**: This arose mainly as a tool to reach immediate goals in solar energy conversion, rapidly becoming an autonomous field of solar energy research. This methodology can ideally be subdivided into the following topics:

   - *Descriptive statistical analysis*, for each place and period of the year, of the main quantities of interest (such as hourly or daily global, diffuse or beam solar irradiation) and statistical modeling of the observed empirical frequency distributions:
   - *Investigation on the statistical relationship* among the main solar radiation components on the one hand (instance, diffuse versus global irradiation and the spatial correlation between simultaneous solar data at different places on the other;
   - *Research on the statistical interrelationship* between the main solar irradiation components and the other available meteorological parameters such as sunshine duration, cloudiness, temperature, etc.
   - *Forecasting of solar radiation values* at a given place or time based on historical data. The statistical forecasting models often constitute a method used in climate prediction. It is also

an appropriate methodology to estimate the parabolic future of a system based on its historical behavior (Badesu, 2008).

Statistical models are considered simpler as they do not require precise information on the composition of the atmosphere. The satellite data over a given area statistically determine the global radiation over that area. On the contrary, the physical models require information about the atmospheric parameters which are essentially used as input to the radiative transfer models which simulate the atmospheric effect on solar radiation (Applasamy, 2011).

2.2 SOLAR RADIATION

Everything in nature emits electromagnetic energy, and solar radiation is energy emitted by the Sun. The extraterrestrial solar radiation is distributed over a wide continuous spectrum ranging from ultraviolet to infrared rays. Depending on the geometry of the earth, its distance from the sun, geographical location of any point on the earth, astronomical coordinates, and the composition of the atmosphere, the incoming irradiation at any given point takes different forms. A significant fraction of the solar radiation is absorbed, scattered and reflected by molecules, aerosols, water vapor and clouds as it passes through the atmosphere and consequently the solar energy balance of the earth remains the same (Sen, 2008). The amount of energy released by the Sun is equal to the amount energy emitted by a furnace at a temperature of approximately 6,000 K (10,340^{o}F) (William et al., 2001).

Radiation is the transfer of energy through electromagnetic waves that move at the speed of light. The velocity of light in a vacuum is approximately 3 x 10^{8} m/s. The time it takes light from the Sun to reach the earth is 8 minutes and 20 seconds. Heat transfer by electromagnetic radiation can travel through empty space. Any body above the temperature of absolute zero (-273.15^{o}C) radiate energy to its surrounding environment. The many different types of radiation are defined by their wavelength. The electromagnetic radiation can vary widely (Beckman, 1991). The amount of solar energy that reaches a unit area at the earth's surface is called the "insolation" or "*solar irradiance"* measured in watts per square meter (W/m^{2}). Solar irradiance is measured instantly and can change with time.

The engineer of solar energy collection systems is keen to know the amount of solar energy collected over a period of time. The total sum is called *solar radiation or irradiation* and the

units are joules per square meter (J/m^2) or watt-hours per square meter (Wh/m^2) (William et al., 2001).

2.2.1 Solar Constant

The sun's radiation is subject to many absorbing, diffusing, and reflecting effects within the earth's atmosphere which is about 10 km average thick and, therefore, it is necessary to know the power density, *i. e.*, watts per square meter per minute on the earth's outer atmosphere and at right angles to the incident radiation. The density defined in this manner is referred to as the *solar constant*. The solar constant and the associated spectrum immediately outside the earth's atmosphere are determined solely by the nature of the radiating sun and the distance between the earth and the sun (Sen, 2008). Solar radiation incident outside the earth's atmosphere is called *extraterrestrial radiation*.

Extraterrestrial radiation fluctuates about 6.9 % during a year (from 1412.0 W/m^2 in January to 1321.0 W/m^2 in July) due to the Earth's varying distance from the Sun. The integration of the extraterrestrial spectrum over all wavelengths defines the **solar constant**. Thus, solar constant represents the rate at which energy reaches the earth's surface from the Sun, usually taken to be 1,388 watts per square metre. The flux density of incoming solar radiation on a unitary surface is perpendicular to the rays at the mean Sun–Earth distance. Since the Sun radiance varies to some extent over short and long periods, the solar constant does not remain steady over time. There is a variation of about ± 1 W/m^2 around the mean solar constant during a typical Sun cycle of 11 years. On average the extraterrestrial irradiance is 1367 W/m^2 (Paulescu et al., 2013).

2.2.2 Extra-terrestrial Solar Spectrum

The spectrum of the sun's radiation just before it passes through the earth's atmosphere is given in Figure 2.1. This is shown along with the solar spectral irradiance for comparison with the spectral irradiance emitted by a blackbody at 6,050 K. Figure 2.1 also gives an integrated value of the spectral solar flux density, showing the cumulative amount of energy radiated at wavelengths between the shortest wavelength and the abscissa value. The data is calculated using 1,353 W/m^2 value of the solar constant.

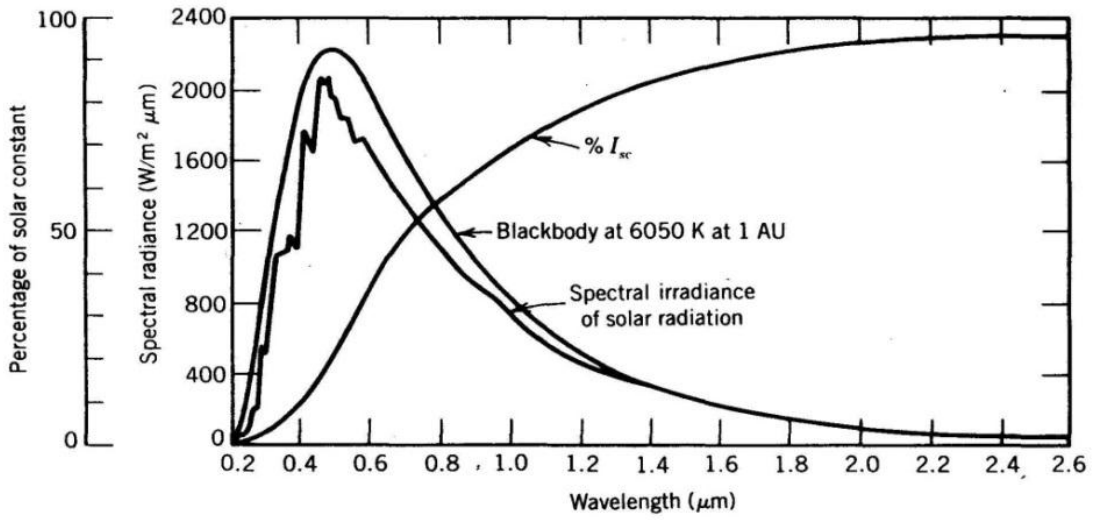

Figure 2.1 Standard extraterrestrial solar spectral irradiance curves. (Thekaekara, 1976).

2.2.3 Extra-terrestrial Solar Irradiance

Because the earth's orbit is slightly elliptical, the intensity of solar radiation received outside the earth's atmosphere varies as the square of the earth-sun distance. Solar irradiance varies by ±3.4 percent with the maximum irradiance occurring at the *perihelion* i.e. earth closest to the sun (January 3-5) and the minimum at the *aphelion* (July 5). This variation may be approximated by:

$$I_O = I_{SC}\left[1 + 0.034\cos\left(\frac{360n}{365.25}\right)\right] \qquad [\mathrm{W/m^2}] \qquad \text{Eqn. 2.1}$$

Where I_o is the extraterrestrial solar irradiance outside the earth's atmosphere and n is the day number (starting at January 1).

An instructional concept, and one often used in solar irradiance models, is that of the extraterrestrial solar irradiance *falling on a horizontal surface*. Consider a flat surface in figure 2.2 just outside the earth's atmosphere and parallel to the earth's surface. When this surface faces the sun (normal to a central ray), the solar irradiance falling on it, will be the maximum possible solar irradiance. If the surface is not normal to the sun, the solar irradiance falling on it will be reduced by the cosine of the angle between the surface normal and a central ray from the sun. This concept is described pictorially in Figure 2.2. It can be seen that the rate of solar energy falling on both surfaces is the same. However, the area of surface *A* is greater than its projection;

hypothetical surface *B*, making the rate of solar energy per unit area (i.e. the solar irradiance), falling on surface *A* less than on surface B.

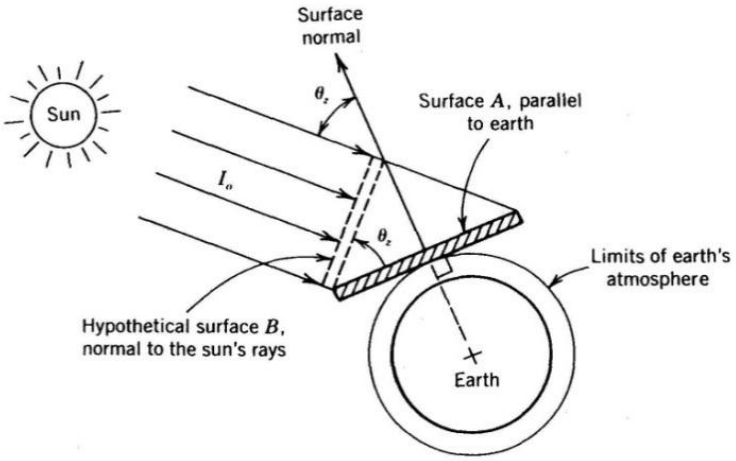

Figure 2.2: The cosine effect as it relates to the concept of extraterrestrial horizontal irradiance1

The extraterrestrial solar irradiance falling on a surface parallel to the ground is:

$$I_{o,h} = I_O \cos\theta_z \qquad [\mathrm{W/m^2}] \qquad \text{Eqn. 2.2}$$

where I_o is the extraterrestrial solar irradiance, and θ_z the angle between the two surfaces, is the solar zenith angle. Reduction of radiation by the cosine of the angle between the solar radiation and a surface normal is called the *cosine effect*.

Because of the cosine effect, the extraterrestrial solar irradiance on a horizontal surface varies cyclically as the earth spins on its axis. The amount of solar radiation received on a horizontal surface outside the atmosphere forms an upper limit to the amount of radiation that will fall on a horizontal surface below the earth's atmosphere. It also describes the cosine effect without the complication of air mass and cloud cover.

2.3 BASIC RADIATION LAWS

The rate at which electromagnetic radiation is emitted by a body is directly related to its temperature. A black body is a body, which emits and absorbs, at any temperature, the maximum possible amount of radiation at any given wavelength. The blackbody is a theoretical concept, which states an upper limit on the emission of radiation in accordance with the second law of

thermodynamics. It is also a standard against which the radiation characteristics of the other media are compared. The emissive power of a blackbody is the amount of energy per unit area per unit time.

2.3.1 Max Planck's Law

A relationship which yields the emissive power of a blackbody at any temperature and wavelength was derived by Max Planck in 1900. Planck's law states:

$$B_\lambda(T) = \frac{2hc^2}{\lambda^5\left(exp\left(\frac{hc}{k_B T\lambda}\right)-1\right)} \qquad \text{Eqn. 2.3}$$

Or in wave number as:

$$B_v(T) = \frac{2hv^3c^2}{exp\left(\frac{hc}{k_B T\lambda}\right)-1} \qquad \text{Eqn. 2.4}$$

Where $B_\lambda(T)$ is monochromatic emissive power of a blackbody ($W/m^2/mm$) at temperature T(K) for the wavelength λ (mm) or wave number (cm^{-1}), and the constants are Plank's constant, h: the Boltzmann constant, k_B and the velocity of light (c)

2.3.2 Stefan-Boltzmann Law

If the body is a perfect emitter (blackbody), the rate at which radiation is given off is proportional to the 4^{th} power of its temperature as measured in degrees Kelvin. This natural phenomenon is described by the Stefan-Boltzmann law:

$$E = \sigma T^4 \qquad \text{Eqn. 2.5}$$

Where $\sigma = 5.67 \times 10^{-8}\ Wm^{-2}k^{-4}$ and T is in Kelvin

Generally, good emitters of radiation also absorb radiation well at specific wavelength bands. This can be confirmed especially with greenhouse gases.

2.3.3 Wien's Law

The wavelength of maximum emission of any body is inversely proportional to its absolute temperature. Therefore, the higher the temperature, the shorter is the wavelength of maximum emission. This is called Wien's law: where T is in Kelvin. The equation 2.5 gives the wavelength

with maximum emission for the sun (5800 K) about $0.5\mu m$, while the wavelength with maximum emission for the Earth (288 K) is approximately 10.0 μm.

Wien's Law

$$\lambda_{max} = \frac{C}{T} \qquad \text{Eqn. 2.6}$$

$$C = 2897$$

where T is in Kelvin.

The gases of the atmosphere are relatively good absorbers of long wave radiation and thus absorb the energy emitted by the Earth's surface. The absorbed radiation is re-emitted in all directions but some downward toward the surface as long wave atmospheric counter-radiation keeping near surfaces temperatures warmer than they would be without this blanket of gases. This is known as the "greenhouse effect".

2.3.4 Inverse Square Law

The amount of radiation passing through a specific area is inversely proportional to the square of the distance of that area from the energy source. This is called the inverse square law.

$$Intensity = \frac{I}{d^2} \qquad \text{Eqn. 2.7}$$

Where I is the intensity of radiation at one end and d is the distance traveled by the radiation from the Sun is lessened by the inverse square law as it reaches further and further away from the Sun. So the further away that a planet is from the Sun then the less radiation it receives. What happens to that radiation depends on whether the planet has an atmosphere, whether the atmosphere contains clouds and how the clouds, or the surface, reflect the radiation.

2.4 SOLAR RADIATION DERIVED FROM SATELLITE OBSERVATION

Generally, solar radiation is measured using networks of meteorological stations. Costs for installation and maintenance of networks are usually very high as result most national networks comprise of only few stations. Therefore, the availability of measured solar radiation data has proved to be spatially inadequate for many applications. Mapping solar radiation by way of interpolation and/ or extrapolation of measurements is possible but usually leads to large errors,

except for dense networks (Journ´ee, 2010). Satellite data can produce a reliable database over large regions on a 0.1^{o} grid (about 10 by 10 km in the Pacific Northwest). However, satellite measurements lack the accuracy and short time interval data necessary for many engineering and site specific studies. Taken together, ground-based and satellite-derived solar radiation measurements create a comprehensive solar radiation database (Vignola, 2006).

In the last decades, a number of methods for estimating solar radiation from satellite data have been developed. Most of the methods for deriving solar radiation from satellite observations employ meteorological geostationary satellite images. The geostationary satellites, orbiting at about 36,000 km, can offer a temporal resolution of up to 15 min and a spatial resolution of up to 1 km. The meteorological satellites collect images over a large area and with high time resolution allowing identification and forecasting the clouds evolution. This information is further processed, leading to the prediction of spatial variability of solar radiation at the ground level. Compared to ground measurements, satellite-derived hourly irradiation has been shown to be the most accurate option for locations that are further away with more than 25 km from a ground station. Thus, processing data collected by satellites can be a viable solution for forecasting solar radiation at the ground, aiming to properly operate the power grid (Paulescu, et al., 2013).

The advantages of space observations emanate from several factors such as:

- Synoptic view of large areas, bringing out the inter-relations of processes of different spatial scales.
- Frequent observations from geostationary satellites provide continuous monitoring while polar orbiting satellites give typically twice daily coverage; such data is relevant for study of weather system dynamics.
- The inherent spatial averaging is more representative than the point in-situ observations and readily usable for weather prediction models.
- High level of uniformity of space observations overcomes the problem of inter-calibration needed for ground based instruments.
- Filling of gaps in observations; space data covers large oceanic areas and inaccessible and remote land areas, thus giving global coverage.

- New types of data and observations; parameters such as sea surface (skin) temperature, sea surface wind stress, sea level, cloud liquid water content, radiation balance, aerosol are some of the unique parameters provided only by satellites.
- Simultaneous observation of several dynamic parameters provided by different sensors in same platform facilitates study of inter-relationships and knowledge of processes (e.g. Sea surface temperature and deep convection, cloud development and radiative forcing) (Kalsi.S.R, 2003).

2.4.1 Satellite Based Models for Deriving Solar Radiation

Geostationary meteorological satellites record backscattered solar radiation from the earth-atmosphere system at high temporal frequencies, therefore providing a means to estimate surface solar irradiance. In the past 30 years, some models have been proposed to derive solar radiation from satellite data. These models have different degrees of complexity and accuracy (Janjai et al, 2013). The tasks involved in determining the solar radiation from satellite imageries is as described in Figure 2.3.

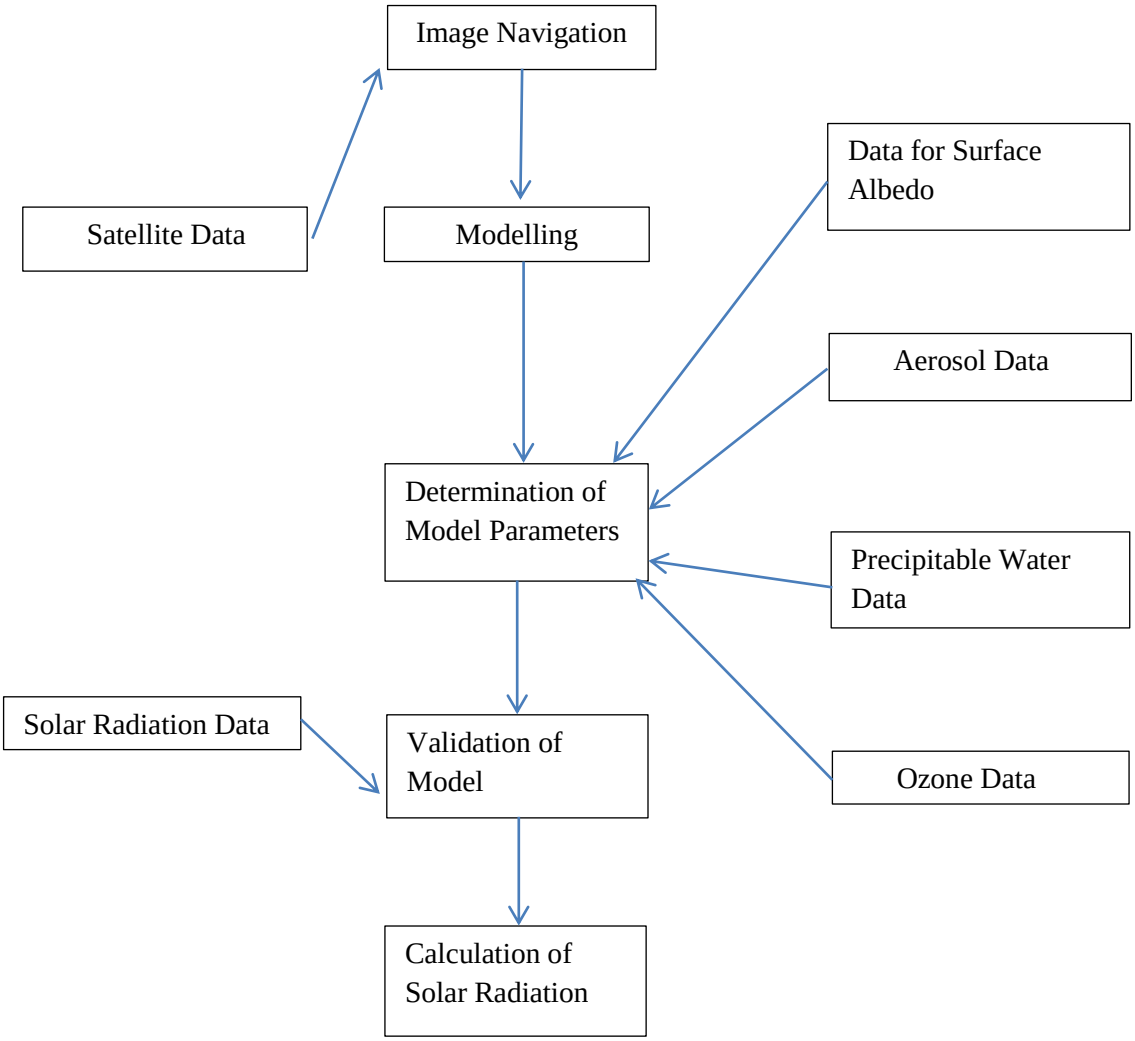

Figure 2.3 Schematic diagram of the method for calculating solar radiation

The equation that governs the satellite-based models is derived from the interaction of extraterrestrial radiation with the earth-atmosphere system. This way, a part of extraterrestrial radiation (G_{ext}) is reflected (G_r), other part is absorbed (G_a), and the remaining (G_g) is absorbed by the ground. Enclosed in brackets is the notation for the corresponding energy flux density. The energy conservation gives:

$$G_{ext} = G_r + G_a + G_g \qquad \text{Eqn. 2.8}$$

Expressing the energy absorbed by the ground as a function of global solar irradiance $G_\rho = (1-\rho)G$, where ρ is the surface albedo, Eqn. 2.8 becomes:

$$G = \frac{1}{1-\rho}(G_{ext} - G_r - G_a) \qquad \text{Eqn. 2.9}$$

Equation (2.9) represents the basis of all models developed for retrieving solar irradiance from satellite images. In Eq. (2.8), G_{ext} is well defined by astronomical equations and G_r is measured by the satellite radiometer. The methods for estimating ground data differ by the way in which G_a and ρ are estimated. The three models commonly used are: Heliosat model; Operational Model and Janjai Model.

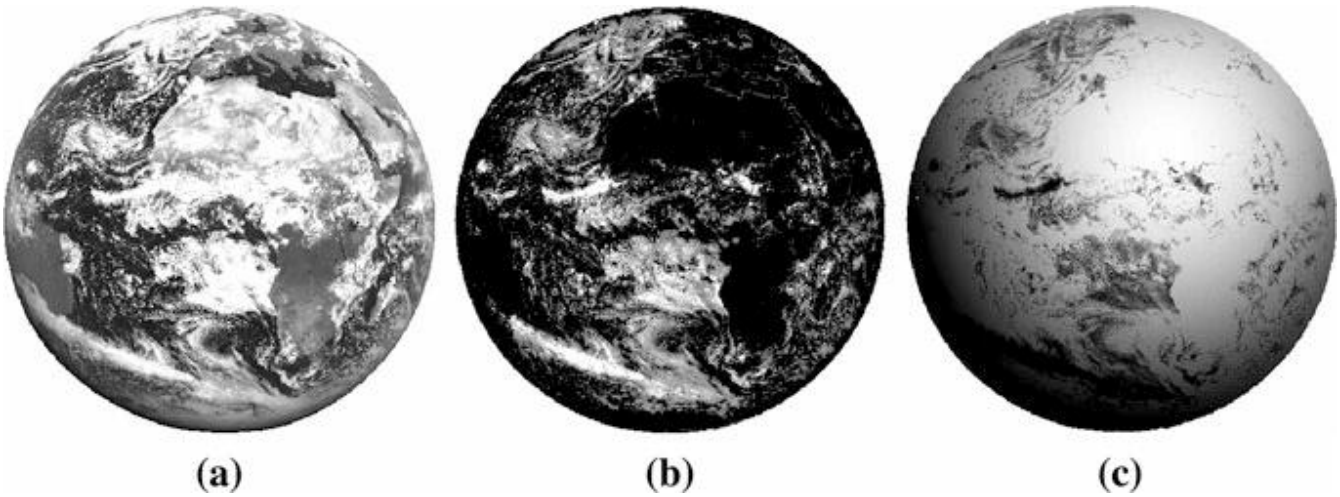

Figure 2.4 Illustration of the processed images by using the Helisat-2 model (http:// www.helioclim.org/heliosat/): (a) raw meteosat data (August 1, 1992, 11h30). (b) Derived cloud cover index. (c) Derived hourly solar global irradiation. Image courtesy Lucien Wald

2.5 PREVIOUS RESEARCHES IN SOLAR RADIATION MODELLING

The need for insolation models has been acknowledged for some time now to design a solar energy system properly for areas lacking insolation data. The first and mostly used insolation model by Moon was published in 1940. This model predicts the direct, diffuse, and global insolation under cloudy sky conditions considering the effect of water vapor absorption. In 1978–1979 Atwater and Ball published the direct and global insolation models under cloudy sky conditions considering the effect of water vapor and oxygen absorptions (Safaripour et al., 2011).

A number of countries the world over have correlated measured solar radiation with meteorological parameters to develop models that predict solar radiation for all locations in such countries. Others have used already developed models like Angstrom type formula to determine constants that will help to estimate solar radiation.

Angstrom-type empirical radiation models based on sunshine hours were used to predict solar radiation data in Egypt. The measured data of the monthly average global solar radiation on a horizontal earth's surface and the number of bright sunshine hours for five locations in Egypt were analyzed. The selected locations represented the various weather conditions of Egypt. The regression constants for the first, second and third order Angström type correlations for each location had been calculated using the method of regression analysis. The values obtained for the RMSE, MBE and the MPE indicated that the second and third order Angström type correlations did not improve the accuracy of estimation of global radiation. Therefore, the measured data available for the selected locations were combined and a first order correlation has been proposed for all Egypt. Comparisons between measured and calculated global radiation indicated that all Egypt correlation is applicable for any location of Egypt and may be extended outside Egypt for places which have the same values of the maximum clearness index ($a + b$). The proposed first order correlations are able to predict the global radiation with percentage error for a single month never exceeding ± 10% in any of the locations (El-Sebaii et al., 2005). Again correlated global solar radiation measurements on a horizontal surface with mean daily maximum temperature, mean daily relative humidity, mean daily sea level pressure, mean daily vapor pressure, and hours of bright sunshine for selected locations over Egypt. The values of correlation coefficients vary from 89% to 99% and the errors of estimation are between 0.01 and 0.04 (Trabea et al., 2000).

In Iraq, estimations of global solar radiation based on a model of using normalized clearness index and normalized sunshine duration for a period of more than 17 years for Haditha, Beji and Samara, for each climatological station were established. The monthly average total solar radiation was also estimated. The reliability index of the calculation varies from 2.1 to 2.9 percent. For the diffuse radiation the Klien method was adapted and the estimations depended on the clearness index as a known and easy method developed for its measurements. The overall results show that for Haditha, the received radiation on the plane surface is higher than for Beji

and Samara while the diffuse radiation behaved conversely in Samara showing the highest value (Fayadh et al., 2010).

The correlation of global solar radiation at Yola in Nigeria was carried out using Angstrom model to estimate the local solar radiation based on the available climatic parameters of sunshine hours (Medugu, 2011).

Solar radiation studies have been carried out to assess the feasibility of solar energy utilization at Hyderabad, Sindh, Pakistan. The result obtained shows the variation of Direct and Diffuse component of solar radiation in summer and winter months. The contribution of diffuse solar radiation is high during the monsoon months (July and August) whereas sky condition is clear during winter months. From the estimated values it is found that with the exception of monsoon months, solar energy can be utilized very efficiently throughout the year (Akhlaque et al., 2009).

M.H Safaripour and M.A Mehrabia predicated the direct, diffuse and global radiation on a horizontal Surface and compared that with real data in Iran. The work dealt with the computation of solar radiation flux at the surface of the earth in areas with no solar radiation measurements, but climatological data available. Simple analytical models from literature were calibrated, and linear regression relations were developed for diffuse, and global solar radiation. The measured data for the average monthly global and diffuse irradiation in Kerman, Iran were compared to the calculated results from the existing models. The data was further compared to values calculated with a linear model using seven relevant parameters. The results indicated that the linear model was better to predict irradiation data in most parts of Iran (Safaripour et al., 2011).

Global Solar Radiation measurements on a horizontal surface, mean daily maximum temperature, mean daily relative humidity, mean daily sea level pressure, mean daily vapor pressure, and hours of bright sunshine, were presented, analyzed, arranged in tables and graphs and discussed for selected locations with different weather conditions over Egypt. A correlation between the measurements of global solar radiation and the meteorological parameters were given for the considered locations. The common relationship for all Egypt was also estimated (El-Sebaii et al,. 2005).

In Malawi, by making use of sunshine-hours data recorded at six selected meteorological stations, namely: Salima, Makoka, Karonga, Bolero, Chileka and Mzimba over the period 1991-

1995, a set of Angstrom constants were obtained and averaged in order to develop the linear regression model. This model has potential for generating ground observation data of solar radiation at any given location in the country using sunshine hours as the only required input (Salima et al., 2012). First order and second order Angstrom model coefficients were obtained for Masvingo and Makoholi locations in Zimbabwe. This was achieved by way of using Long term average ground measurements of sunshine hours and global horizontal solar radiation from the meteorological services were used as input data. Monthly average values of the clearness index and the fraction of sunshine hours were determined. Regression analysis was used to determine the first and second order Angstrom model coefficients for the two areas. The estimates from the developed models were compared against measured values and results were in agreement to $\pm$ 5% (Mapurisa et al., 2013).

According to Nasitwitwi, the global solar radiation at Lusaka, Zambia measured over a wide range of meteorological conditions is influenced by aerosols and other atmospheric controls on cloudless-sky. Houghton's radiation model, was applied to a savanna landscape characterized by tropical atmospheric dynamics and pyrogenic aerosols produced by anthropogenic biomass burning. Angstrom-type empirical radiation models based on sunshine hours were earlier utilized to provide radiation data in Zambia without validation against actual measurements (Nasitwitwi et al., 2000). Subsequent work refined this model using Zambian data. Further, Jain proposed regional coefficients of the Angstrom-type radiation model applicable to all locations in Zambia. Errors in all these modeling procedures were due largely to the low accuracy of radiation and sunshine instrumentation. In addition, Jain isolated substantial unsystematic scatter of regression parameters of the Angstrom model indicative of physical atmospheric processes that were beyond the resolution of Angstrom's model (Jain et al., 1988).

It is generally considered that quality ground measured data are more accurate than satellite-derived values (Kuster, 2008) in that Satellite pixel integrates cloud signal from an area approx. 4 x 5 km while Ground instrument gives a pinpoint measurement (Suri, 2012). However, ground-based measurements and satellite-derived solar radiation data complement each other and are necessary to build a comprehensive solar radiation database. It is impractical to have a high density ground-based solar radiation monitoring network that would give anywhere near the coverage capability of a satellite-derived solar radiation database. In addition the uncertainty of

interpolated data between sites becomes unacceptable as the distance between stations increases (typically in the 20–50 km range). Satellite data can produce a reliable database over large regions on a 0.1 degree grid (about 10 by 10 km in the Pacific Northwest). However, satellite measurements lack the accuracy and short time interval data necessary for many engineering and site specific studies (Vignola, 2006).

2.6 CRITIQUE OF THE THEORY AND RESEARCH LITERATURE

In many developing countries, solar radiation measurements are not easily available for many locations due to cost, maintenance and calibration requirements of measuring equipment. Therefore, empirical-analytical relationships are developed and used to predict solar radiations. In Zambia previous researchers only used **sunshine hours as** in Angstrom model, to propose models that can predict mean monthly daily global solar radiation. However, in this study a number of factors affecting solar radiations reaching the horizontal surface are considered in the development of mathematical models to improve the accuracy and subsequently the database that shall be generated.

The satellite-derived solar radiations for selected locations were compared with the ground measured data to ascertain the reliability of data.

CHAPTER 3 METHODOLOGY

3.1 INTRODUCTION

There are two methods through which solar radiation energy data can be obtained. The first method, which is more accurate, is to measure directly solar radiation components using Pyranometers and Pyrheliometers (El-Sebaii et al., 2005). Consistent measurements of diffuse solar energy and the global solar radiation incident on a horizontal earth's surface are usually undertaken by national agencies, which are the national meteorological offices in many countries. At several locations, a Pyrheliometer with a fast-response multi-junction thermopile is used to measure direct or beam irradiation. Diffuse irradiance is measured at a station by placing a shadow band over a Pyranometer (Sen, 2008).

The second approach relies on empirical-analytical relationships that can predict the solar radiation components as a function of clear sky conditions, latitude, hours of measured sunshine, zenith angle, time, altitude, etc. This approach can be used in locations with similar meteorological and geographical characteristics where measured data on solar radiation energy is not available due to limited coverage of radiation measuring networks (El-Sebaii et al., 2005). This method uses regression analysis and can be applied to estimate solar radiation to most parts of Zambia where it is not measured.

Regression analysis is a statistical tool for the establishment of relationships between variables. Usually, the investigator seeks to ascertain the effect of one variable upon another. To explore such issues, the data of the underlying variables of interest is assembled and regression analysis is employed to predict the quantitative effect of the variables upon the variable that they influence. What is also typically assessed is the "statistical significance" of the estimated relationships, that is, the degree of confidence that the true relationship is close to the estimated relationship, (Sykes, 1986).

3.2 SOLAR RADIATION ON HORIZONTAL SURFACE

At any point in time, the solar radiation outside the atmosphere (I_o) incident on a horizontal plane is:

$$I_o = I_{sc}\left[1.0 + 0.033\cos\left(\frac{360n}{365}\right)\right]\cos\theta_z \qquad \text{Eqn. 3.1}$$

Where I_{sc} is the solar constant and n is the day of the year. The recommended average days for each month and values of n by month are given in Table 3.1.

Table 3.1 Recommended Average days for Months and Values of n each Months

		For the average day of the month		
Month	n for i^{th} day of month	Date	Day of the year n	Declination
January	i	17	17	-20.9
February	$31 + i$	16	47	-13
March	$59 + i$	16	75	-2.4
April	$90 + i$	15	105	9.4
May	$120 + i$	15	135	18.8
June	$151 + i$	11	162	23.1
July	$181 + i$	17	198	21.2
August	$212 + i$	16	228	13.5
September	$243 + i$	15	258	2.2
October	$273 + i$	15	288	-9.6
November	$304 + i$	14	318	-18.9
December	$334 + i$	10	344	-23

Source: From Duffe and Beckman, 1991

Substitution of the expression for $\cos\theta_z$, from equation above gives,

$$I_o = I_{sc}\left[1.0 + 0.033\cos\left(\frac{360n}{365}\right)\right]\cos\emptyset\cos\delta\cos\omega + \sin\delta\sin\emptyset \qquad \text{Eqn. 3.2}$$

It is often required to have the integrated daily extraterrestrial radiation on a horizontal surface, H_o, for the calculations of daily solar radiation. This can be obtained by integrating equation 3.2 over the period from sunrise to sunset.

If I_{sc} is in Watts/m^2 and H_o in Joules/m^2 then

$$H_o = \frac{24\ x\ 3600}{\pi} I_{sc}\left[1.0 + 0.033\cos\left(\frac{360n}{365}\right)\right]\ x\ \left(cos\emptyset cos\delta\sin\omega_s + \left(\frac{2\pi\omega_s}{360}\right)\sin\emptyset\sin\delta\right)$$

Eqn.3.3

where ω_s is the sunset hour angle in degrees.

H_o, the mean monthly daily extraterrestrial radiation can be obtained from the above expression by using day numbers from table 3.1. The terrestrial radiation on horizontal surface for an hour period can be calculated by integrating equation 3.2 for a period defined by hour angles ω_1 and ω_2 which define an hour (where ω_2 is larger):

$$I_o = \frac{24\,x\,3600}{\pi} I_{sc}\left[1.0 + 0.033\cos\left(\frac{360n}{365}\right)\right]\, x\, \left(cos\emptyset cos\delta(\sin\omega_2 - \sin\omega_1) + \left(\frac{2\pi(\omega_2-\omega_1)}{360}\right)\sin\emptyset\sin\delta\right),$$ (Tiwari 2013). Eqn. 3.4

where θ_z is the solar zenith angle, ω is the hour angle, ω_s is the sunset angle and $\emptyset$ is the latitude angle (Tiwari, 2013).

3.3 SUMMARY OF THE SOLUTION

In this research, the general procedure for developing a mathematical model for solar radiations is achieved by correlating the measured data sets of solar radiations and geographical, geometrical, astronomical and meteorological (GGAM) parameters for all the locations but limited to where solar radiation is measured in Zambia. Using linear regression and starting with one GGAM parameter, the equation takes the form:

$$y = a + bx$$ Eqn. 3.5

where a and b are regression coefficients and x is the correlated parameter.

As the number of GGAM parameters increase, the correlation becomes a multiple linear regression taking the following form:

$$y = a + bx_1 + cx_2 + dx_3 + ex_4 + fx_5 + gx_6 + hx_7 + ix_8 + jx_9 + kx_{10}$$ Eqn. 3.6

Where:

i. $a, b, c, d, e, f, g, h\ and\ i$ are regression coefficients and
ii. $x_1, x_2, \ldots x_{10}$ are correlated parameters.

The proposed solar radiation models take the form as:

$$H = a + b\sin\delta + cH_o + d\,{}^{n}/_{N} + eR_h + fT_{max} + gT_{dp,max} + hP + iC$$ Eqn. 3.7

Where:

H_o is the monthly mean daily extraterrestrial solar radiation,

n/N is the monthly average daily ratio of sunshine duration,

R_h is the mean daily relative humidity,

T_{max} is the monthly mean daily maximum air temperature

$T_{dp,max}$ is the monthly mean daily maximum dew point temperature

P is the monthly mean daily atmospheric pressure

$Sin\delta$ is the sine of the solar declination angle

C is the monthly mean of the cloud cover,

H is the predicated monthly mean daily global solar radiations

3.4 SOLAR RADIATIONS AND GGAM DATA SETS

The nature of solar radiation and GGAM data sets collected, combined and used in this work were for the years running from 1930 through 2013 and encompassing different climatological conditions for the selected regions of Zambia. Figure 3.1 below shows the climatological zones for Zambia.

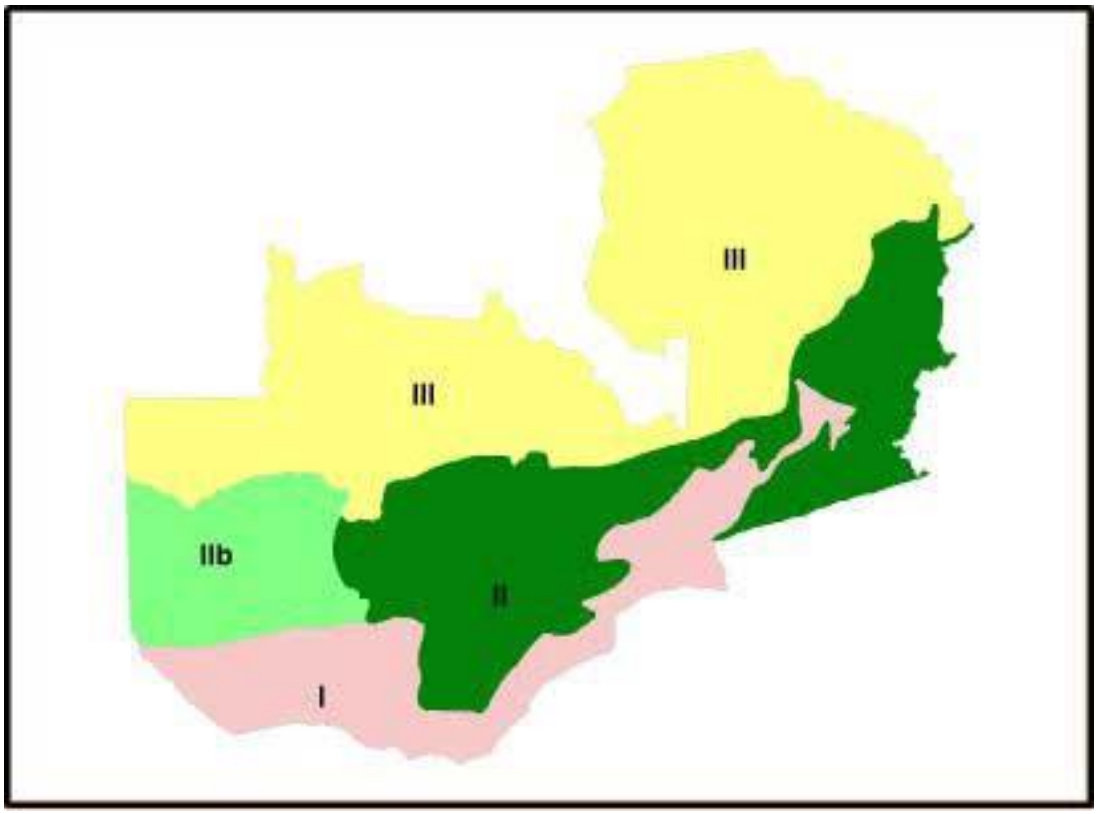

Figure 3.1: Zambia agro-ecological regions I, IIa, IIb and III

Sources: CFA, Zambia Branch homepage

Key

Region	**Annual Rainfall**
I	Less than 700 mm
IIa	800 - 1000 mm
IIb	800 - 1000 mm
III	1000 - 1500 mm

The Zambia Meteorological Department (ZMD) in the Ministry of Transport and Communications measured the data for the following locations namely; Kasama, Livingstone Lusaka, Mansa, Mfuwe, Mongu, and Ndola. Livingstone and Mongu are located in the south of Zambia, Mfuwe in the east, Lusaka and Ndola in the middle while Mansa and Kasama are in the

northern part of Zambia. The data sets for the daily measurements of GGAM parameters and global solar radiations collected for each site were:

(i) cloud cover;
(ii) sunshine hours;
(iii) dew point temperature;
(iv) humidity;
(v) maximum temperature;
(vi) atmospheric pressure;
(vii) solar radiation;

The measured data by ZMD was given to the author strictly for the purpose of carrying out this research and due to the bulk nature of it, a Compact Disc is provided at the back of this thesis.

3.5 SATELLITE DERIVED SOLAR RADIATION DATABASES

There are a number of solar radiation web-based databases from satellite imagery available which include among others; SOLEMI (DLR), NASA-SSE (NASA), PVGIS (JRC), Satellite Application Facility (SAF), SATEL-LIGHT, ESRA (SoDa, 2004). However, depending on the coverage, for instance, the Heliosat and/or the SolarGiS groups produce estimates from the Meteosat series of geostationary satellites that cover Zambia.

3.5.1 Heliosat

The Heliosat method converts images acquired by meteorological geostationary satellites, such as Meteosat (Europe), GOES (USA) or GMS (Japan), into data and maps of solar radiation received at ground level. By using the methods Heliosat, the databases HelioClim of solar radiation (irradiation or irradiance), were and are, created by processing Meteosat images.

HelioClim is a family of databases which comprise irradiation and solar irradiance values available at ground level. HelioClim covers Africa, Europe, the Mediterranean Basin, the Atlantic Ocean and part of the Indian Ocean. Mines Paristech - Armines receive Meteosat data from Eumetsat and process them in real time. Mines Paristech - Armines produce the databases HelioClim, which can be accessed through the SoDa Service (meteorology - observations). There are presently three databases in the HelioClim family of the Mines ParisTech - Armines: HC-1, HC-2 and HC-3. Work is on-going on the most recent database HC-3. An improved method of

Heliosat-4 is under preparation, to process Meteosat images. It is intended to create the database HC-4 (SoDa, 2004).

3.5.2 SolarGIS

SolarGIS is a geographical information system created to mitigate the needs of the solar energy industry. It combines solar resource and meteorological data with tools for planning and performance monitoring of solar energy systems.

In SolarGIS, uncertainty of Global Horizontal Irradiation (GHI) yearly summaries is typically lower than ±3.5 percent with a probability of occurrence 80 percent for 89 validation sites. In mountains, tropical humid climates, complex coastal zones, high latitudes, snow regions, and regions with high aerosol concentrations (air pollution) the uncertainty can be as high as ±7.0 percent. In very extreme cases higher deviations were observed.

Uncertainty for Direct Normal irradiation (DNI) yearly summaries is typically lower than ±7 percent with a probability of occurrence 80 percent for 48 validation sites. In more complex geographies, uncertainty of yearly DNI can be as high as ±12 percent. Deviations up to 15 percent from local measurements have been sporadically observed, especially in regions where aerosol content is high and dynamically changing, in humid tropical regions, high latitudes, high mountains, snow regions, complex deserts with occasional occurrence of snow and water, urbanized and industrialized areas. High uncertainty is also considered in regions with limited availability of high-quality ground measurements.

3.5.3 NASA Surface Meteorology and Solar Energy (SMSE 2012)

Solar radiation data for the selected sites in Zambia from satellite data, provided by web-based systems and databases, were obtained from **NASA Surface Meteorology and Solar Energy (SMSE 2012)** for comparison with ground measured data**.** NASA, through its' Earth science research program, has for a long time supported satellite systems and research to provide data which is important to the study of climate and climate processes. This data include long-term estimations of meteorological quantities and surface solar energy fluxes (SSE Release 6.0, 2012).

3.6 ADVANCED COMPUTER PROGRAM MATLAB 2011B

The data collected from ZMD was analysed, organized and presented in tabular and graphical forms to make practical sense and subsequently used in the Regression Analysis to develop the solar radiation models. The advanced computer program MATLAB2011b was used to determine the values of parameters (regression coefficients) for the equations (Eqn. 3.7), whose form was specified and cause the equation to best fit a set of data values.

MATLAB (MATrix LABoratory) is a tool for numerical computation and visualization. It allows matrix manipulations, plotting of functions and data, implementation of algorithms, creation of user interfaces, and interfacing with programs written in other languages, including C, C++, Java, and Fortran. So Matlab is a program that manipulates array-based data and is generally fast to write and run in MATLAB.

3.6.1 Linear Regression in Matlab

MATLAB allows one to model data using linear regression. A *model* is a relationship between independent and dependent variables. Linear regression produces a model that has a linear relationship in the model coefficients. The commonest linear regression type is the least-squares *fit*, that can fit both polynomials and lines.

3.6.2 Residuals and Goodness of Fit

Residuals are defined as the difference between the *measured* values of the dependent variable and the values that are *predicted* by the model. When fitting a model, that is appropriate for some particular data, the residuals approximate independent random errors. To calculate fit parameters for a linear model, MATLAB minimizes the sum of the squares of the residuals to produce a good fit. This is called a least-squares fit.

3.6.3 Correlation Analysis

Before modeling the relationship between pairs of measured values, it is a good practice to perform correlation analysis in order to establish if a relationship exists between these quantities. *Correlation* is a method for establishing the degree of probability that a linear relationship exists between two measured quantities. When there is no correlation between the two quantities, then there is no tendency for the values of one quantity to increase or decrease with the values of the

second quantity. MATLAB provides three functions for computing correlation coefficients and covariance. In typical data analysis applications, the mostly sought is the degree of relationship between variables where one needs only to calculate correlation coefficients. That is, it is not necessary to calculate the covariance independently (Mathworks, 2007).

3.7 MEAN OF ABSOLUTE DEVIATIONS, MEAN BIAS ERROR, AND ROOT MEAN SQUARE ERROR

The accuracy of the solar radiation mathematical models is important not only in the final stages of projects, but particularly in the initial stages prior to any systematic model construction work. In order to gain insight into the performance evaluation of a model, mean bias error (MBE), mean absolute deviation (MAD), and root mean square error (RMSE) shall be defined in sequence as follows:

$$MBE = \frac{1}{n}\sum_{i=1}^{n}(Y_i - \bar{Y}_i) \qquad \text{Eqn. 3.8}$$

$$MAD = \frac{1}{n}\sum_{i=1}^{n}|Y_i - \bar{Y}_i| \qquad \text{Eqn. 3.9}$$

$$RMSE = \frac{1}{n}\left[\sum_{i=1}^{n}(Y_i - \bar{Y}_i)^2\right]^{1/2} \qquad \text{Eqn. 3.10}$$

The MBE is given as the arithmetic average of the errors. If its value is equal to zero, it does not mean that the model yields estimations without error. The MBE provides a measure of the overall trend of a given model, i.e., predominantly over-estimating (positive values) or under-estimating (negative values). However, the smaller the MBE the better is the model result.

On the other hand, in an acceptable model, the MAD value should be as close as possible to zero, but never equal to zero in the solar radiation modeling. The RMSE is similar to the MAD and provides a measure of squared deviations. In statistics, the RMSE of an estimator is the square root of the expected value of the "square of the error". This is the amount with which the model estimate differs from the corresponding measurement. The error occurs because of randomness or the model does not give information that could be used to produce a more accurate estimate (Sen, 2008).

3.8 SAMPLE CALCULATIONS FOR SOLAR RADIATION MODELS

The measured data of global solar radiation and the meteorological parameters, collected from ZMD and provided in the Compact Disc (CD) at the end of the report was analysed and presented Tables 4.3 - 4.10 in Appendix A for all the selected locations in Zambia namely; Kasama, Lusaka, Livingstone, Mansa, Mfuwe, Mongu and Ndola. The data was further processed and analyzed using an advanced computer program Matlab 2011b to obtain the correlation and the regression coefficients *a, b, c, d, e, f, g, h*, and *i* in Eqn. 3.7. The obtained values of correlation coefficients (CC) and the standard errors of estimation (SE) besides the regression coefficients are listed in **Table 4.2** in Chapter 4.

In order to predict the monthly mean daily global solar radiations as in Eqn. 3.7, sine of declination angle ($sin\delta$), monthly mean daily extraterrestrial radiation on a horizontal surface, H_o, and the potential astronomical sunshine hours (or day length) *N*, were determined to make it easier to use the equation. The other equation parameters for each selected location to include; the mean monthly daily relative humidity (R_h), the mean monthly daily maximum air temperature (T_{max}), the mean monthly daily maximum dew point temperature ($T_{dp,max}$), the mean monthly daily atmospheric pressure (P) and the mean monthly of the cloud cover, (C) are provided in tables 4.3 – 4.9 in Appendix A.

i. Sine of declination angle, $sin\delta$

$$\sin\delta = 0.39795\cos[0.98563(n^* - 173)] \text{ or}$$
$$\delta = 23.45\sin[360(284 + n^*)/365]$$

n= day of the year (1, 2, 3… 365). Taking 17 as an average day for January in **Kasama**.

$$\sin\delta = 0.39795\cos 0.98563(-156)$$

$$\boldsymbol{\sin\delta = -0.35695}$$

$$\boldsymbol{\delta = -20.92^o}$$

ii. The monthly mean daily extraterrestrial solar radiation on a horizontal surface, H_o:

The following calculation was carried for day of the month then averaged over the month to provide the **mean daily radiation on a horizontal surface, H_o.** For example taking *n* as 17 for January:

$$H_o = \left\{\frac{24\ x\ I_{sc}}{\pi}\left(cos\emptyset cos\delta \sin\omega_s + \left(\frac{\pi\omega_s}{180}\right)\sin\emptyset \sin\delta\right)\right\} x\ 3.6/1000 \qquad [MJ/m^2]$$

The rate of extraterrestrial solar radiation (solar irradiance) just outside the earth's atmosphere I_0 is calculated by:

$$I_o = \left(1 + 0.033\cos\frac{360n}{365}\right) I_{sc} \qquad [W/m^2]$$

Taking n = 17 for January

I_{sc} = 1367 W/m^2 the solar constant.

$$I_0 = \left(1 + 0.033\cos\frac{360x\ 17}{360}\right) = \underline{\mathbf{1410.2}}\ W/m^2$$

$$\sin\delta = -0.35695$$

Latitude for Kasama $\emptyset = 10.2117$

ω_s = sunset hour angle

The sunset hour angle is given by: $\omega_s = \cos^{-1}(-\tan\emptyset \tan\delta)$

$$\omega_s = \cos^{-1}(-\tan(-20.92)\tan(-10.2117))$$

$$= \cos^{-1}(-0.06886) = \underline{\mathbf{93.90^o}}$$

Therefore,

$$H_o = \left\{24\ x\ 1410.2\ \left(\cos(-10.2117)\cos(-20.92)\sin(93.94) + \left(\frac{\pi x\ 93.94}{180}\right)\sin(-10.2117)\sin(-20.92)\right)\right\} x\ 3.6/1000$$

$$H_o = \underline{\textbf{39.5787 MJ/m}^2}$$

The same above calculation was carried out for all the recommended days as in Table 3.1 to find the average extraterrestrial global solar radiation $\boldsymbol{H_o}$ on a horizontal surface for each month of the year as **39.5787 MJ/m^2** for the month of January for Kasama.

iii. Potential Astronomical Sunshine Hours

N is the potential astronomical sunshine hours (or day length) and *n* is the number of bright sunshine hours.

$$N = \frac{2\omega_s}{15} = 2x\cos^{-1}(-\tan(-10.2117).\tan(+20.92))/15$$

N = **12.5203** hours

Therefore, the sunshine ratio, *n/N* for month of January in Kasama is:

= 4.4281/ 12.5203

= 0.3537

The calculations for each of the selected locations in Zambia were repeated and recorded in Table 4.2

CHAPTER 4 RESULTS AND DISCUSSIONS

4.0 INTRODUCTION

Chapter 4 presents and discusses results in accordance with the objectives of the study. These were to: (1) to collect and analyze GGAM parameters data, ground based and satellite-derived solar radiation data sets at selected sites in Zambia; (2) to use the analyzed data to develop general mathematical models for estimating monthly mean global solar radiation intensities; (3) to use the developed mathematical models to estimate solar radiation model for Zambia where no measured data is available but model parameters obtainable locally.

4.1 GGAM Parameters, ground based and satellite-derived solar radiation data sets at selected sites in Zambia

The development of mathematical models to predict solar radiations on a horizontal surface for Zambia, first and foremost, involved collection of existing historical data for daily measurements of global solar radiation and Geographical, Geometrical, Astronomical and Meteorological (GGAM) parameters. This measured data was collected from Zambia Meteorological Department (ZMD). The analysis procedure required to arrange the data in tabular form and determining correlation coefficients (CC) to ensure that relationships between data sets for global solar radiation and GGAM factors existed.

4.1.1 Variations of measured Global Solar Radiation and GGAM Parameters

Tables A1 – A8 in the Appendix A give data collected, analysed and presented in tabular form for ground measured global solar radiations and GGAM parameters with their CC and standard errors (SE) for the locations namely, Kasama, Livingstone, Lusaka, Mansa, Mfuwe, Mongu and Ndola. While the following plots give the monthly mean variations of the considered parameters over a period of twelve (12) months: maximum temperature (T_{max}); maximum dew point temperature ($T_{dp,\ max}$); global solar radiation (H); sunshine ratio (*n/N)*; relative humidity (R_h); amount of cloud cover (C) and pressure (P) at selected stations in Zambia.

Figures 4.1 – 4.7 show the plots for the monthly mean variations of the considered parameters: maximum temperature; maximum dew point temperature; relative humidity; pressure sunshine hours; cloud cover and ground measured global solar radiation at selected stations in Zambia.

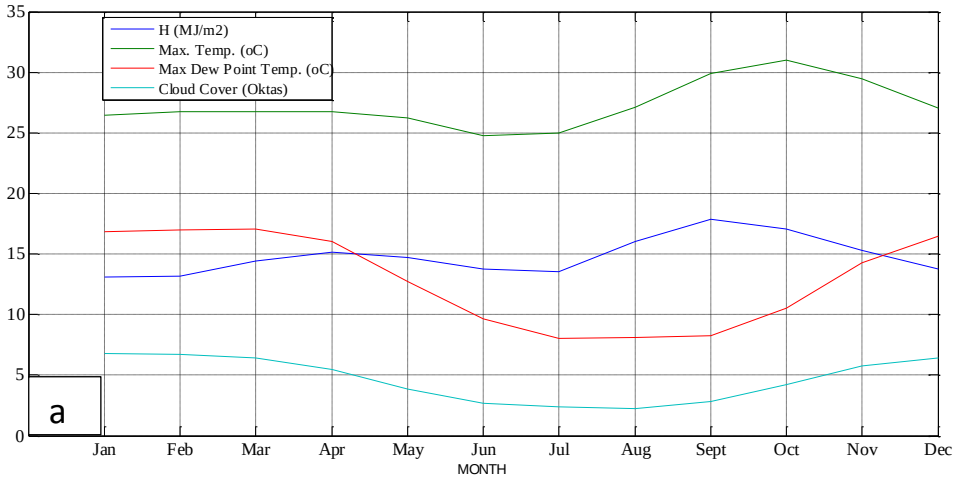
H (MJ/m2)
Max. Temp. (oC)
Max Dew Point Temp. (oC)
Cloud Cover (Oktas)
a
35
30
25
20
15
10
5
0
Jan
Feb
Mar
Apr
May
Jun
Jul
Aug
Sept
Oct
Nov
Dec
MONTH

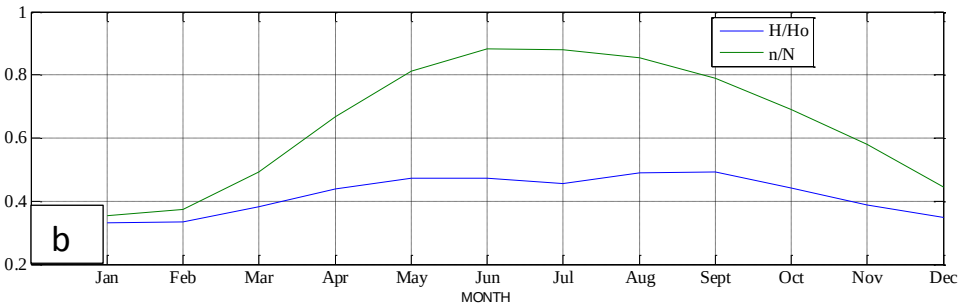
H/Ho
n/N
b
1
0.8
0.6
0.4
0.2
Jan
Feb
Mar
Apr
May
Jun
Jul
Aug
Sept
Oct
Nov
Dec
MONTH

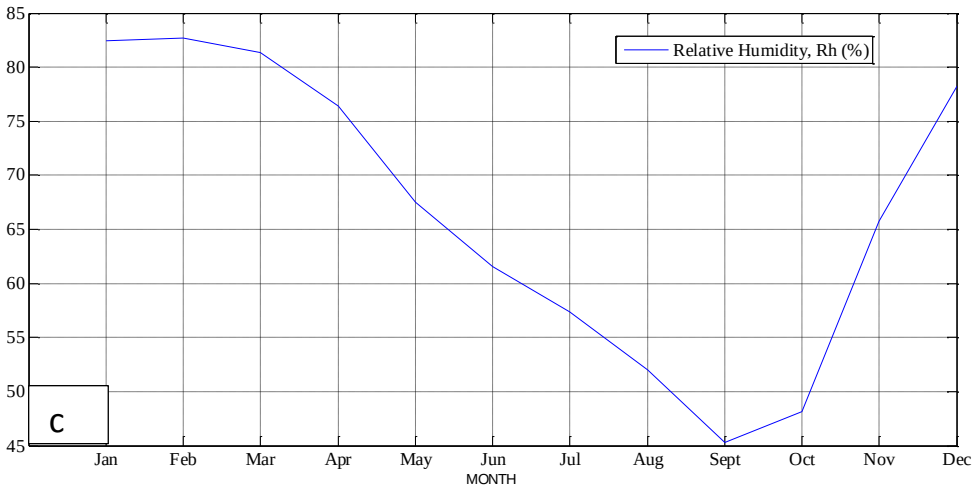
Relative Humidity, Rh (%)
c
85
80
75
70
65
60
55
50
45
Jan
Feb
Mar
Apr
May
Jun
Jul
Aug
Sept
Oct
Nov
Dec
MONTH

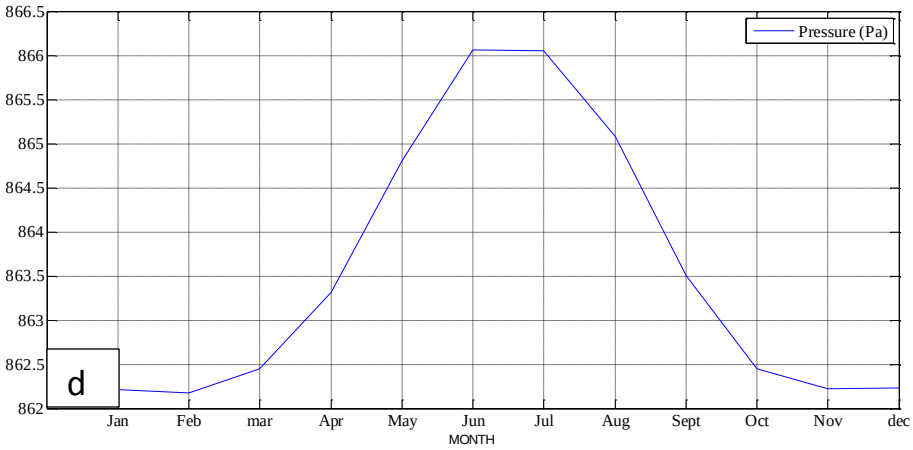

Figure 4.1 Monthly mean daily variations of the considered parameters (a) T_{max}, Cloud Cover C, T_{dpmax} and H_o (b) H/H_o and n/N (c) Relative Humidity, R_h and (d) Pressure at **KASAMA** Station

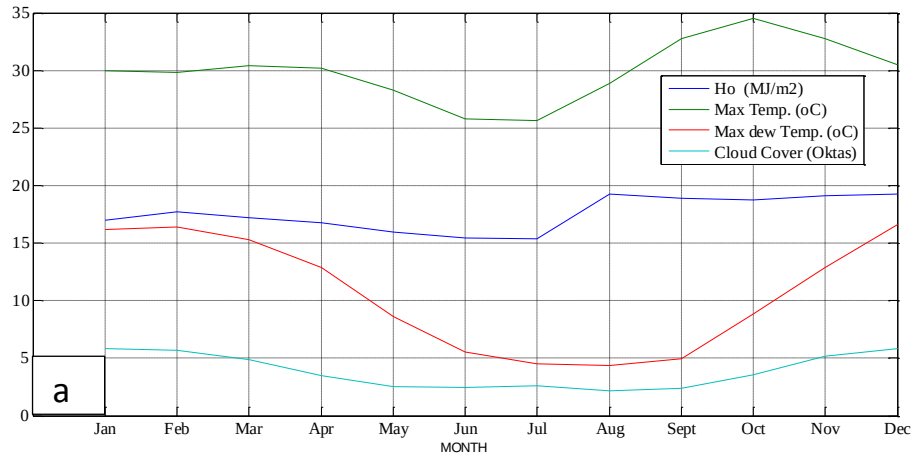

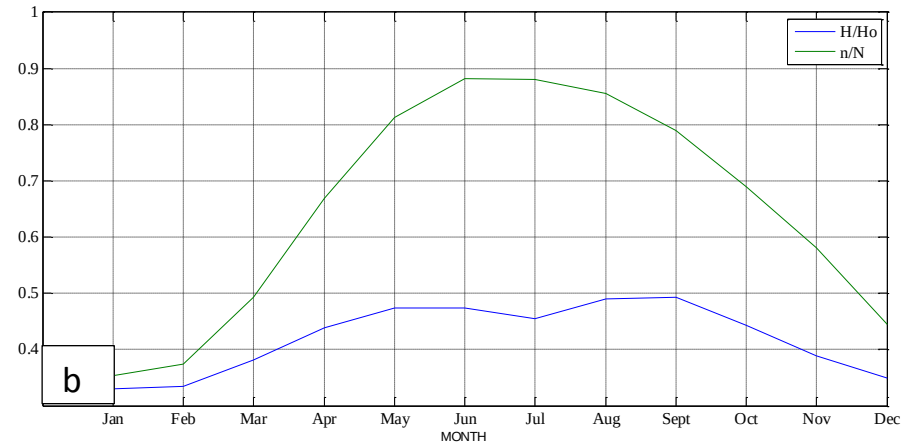

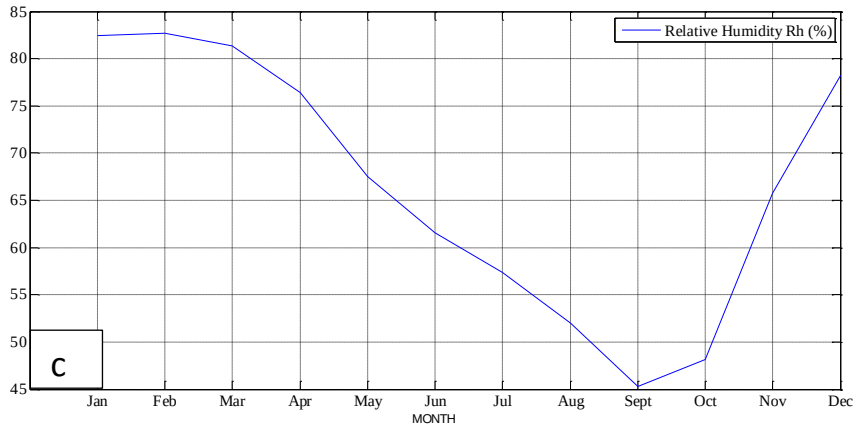

Figure 4.2 Monthly mean daily variations of the considered parameters (a) T_{max} , Cloud Cover C, T_{dpmax} and H_o (b) H/H_o and n/N (c) Relative Humidity, R_h at **LIVINGSTONE** Station

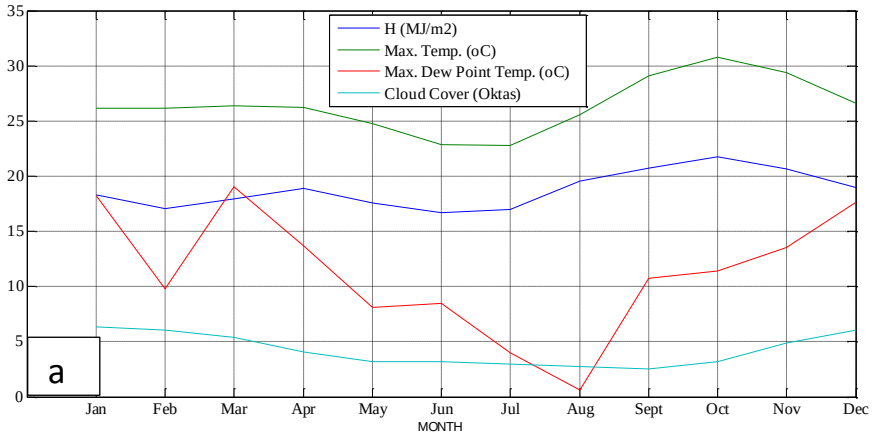

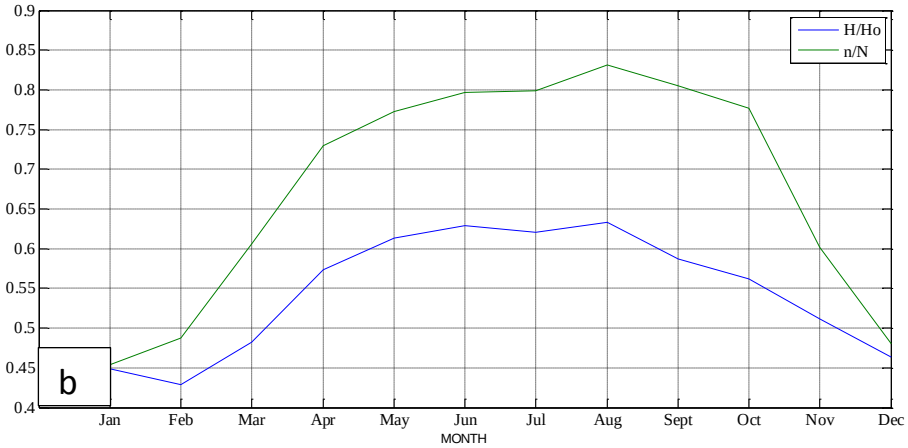

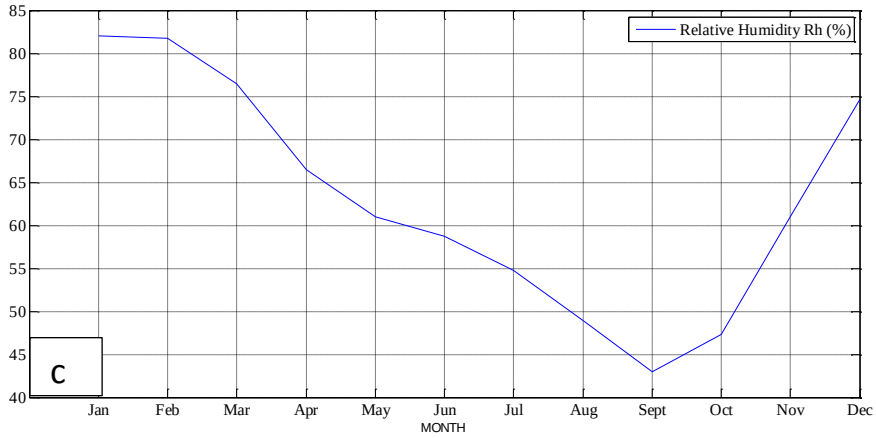

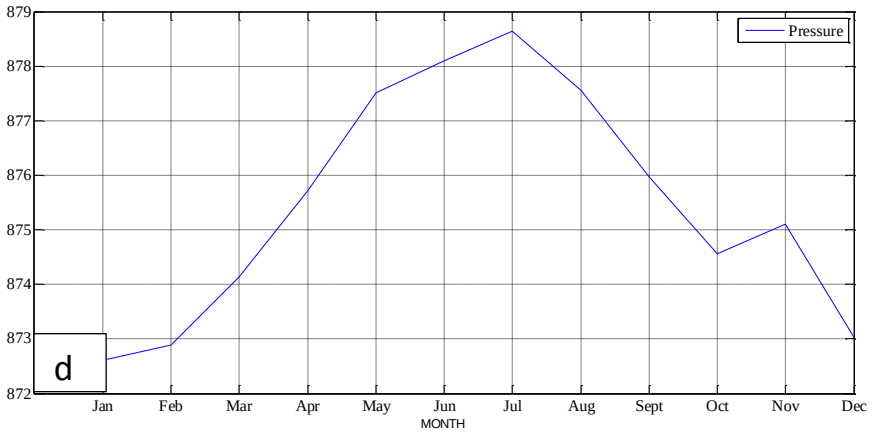

Figure 4.3 Monthly mean daily variations of the considered parameters (a) T_{max}, Cloud Cover C, T_{dpmax} and H_o (b) H/H_o and n/N (c) Relative Humidity, R_h and (d) Pressure at **LUSAKA** Station

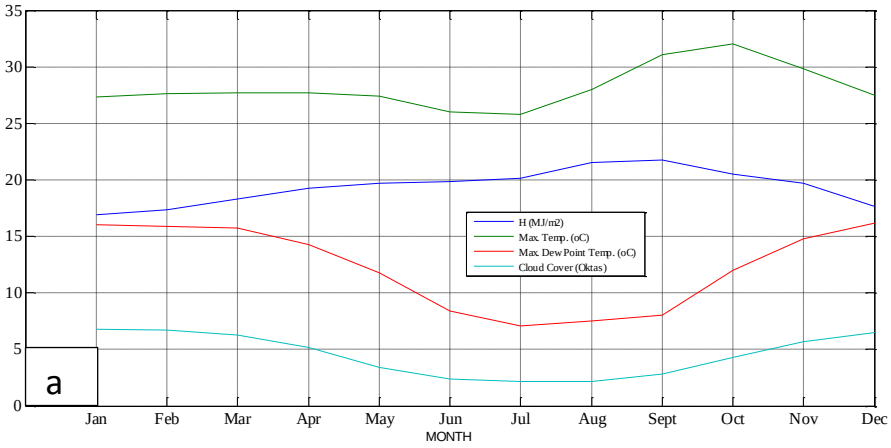

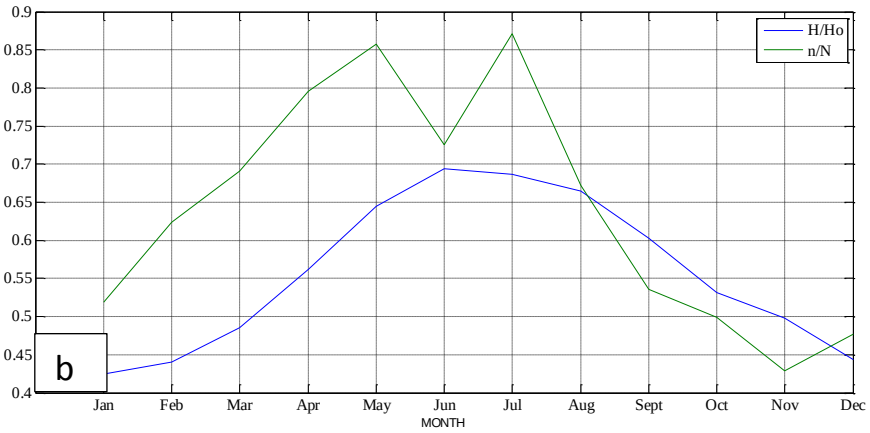

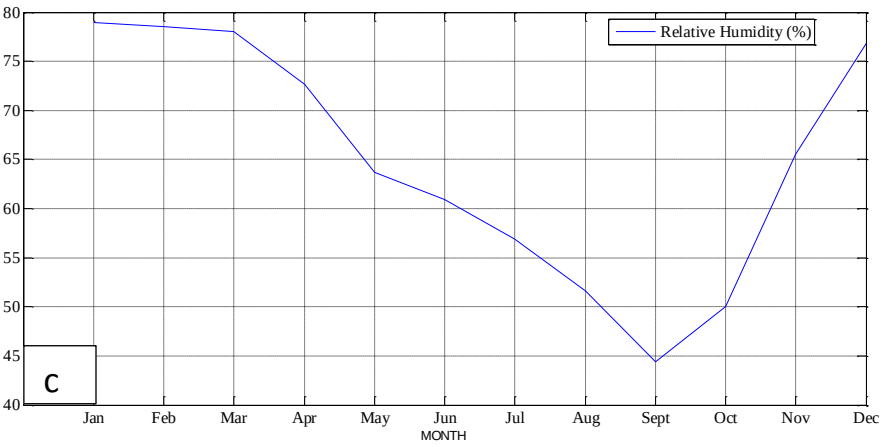

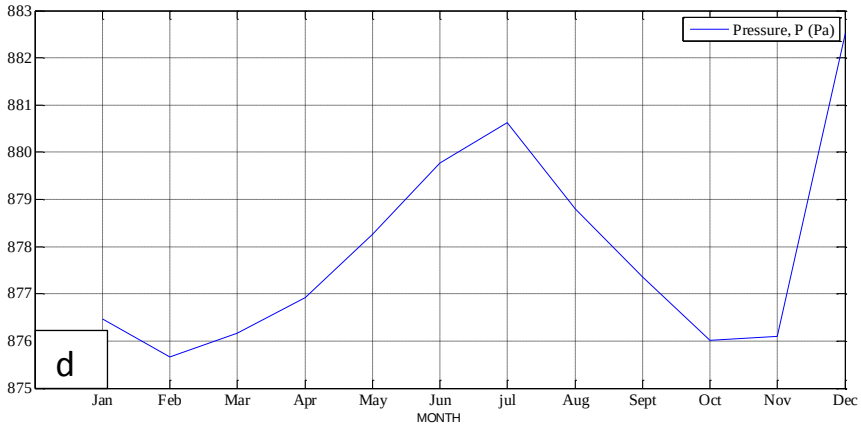

Figure 4.4 Monthly mean daily variations of the considered parameters (a) T_{max}, Cloud Cover C, T_{dpmax} and H_o (b) H/H_o and n/N (c) Relative Humidity, R_h and (d) Pressure at **MANSA** Station

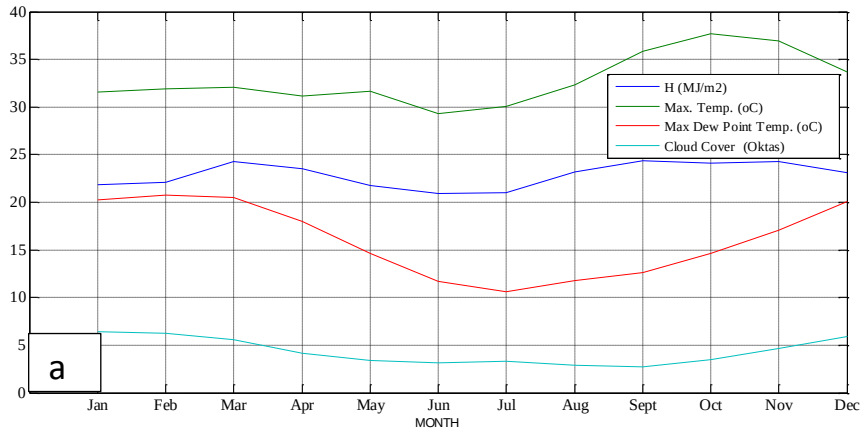
H (MJ/m2)
Max. Temp. (oC)
Max Dew Point Temp. (oC)
Cloud Cover (Oktas)
a
MONTH

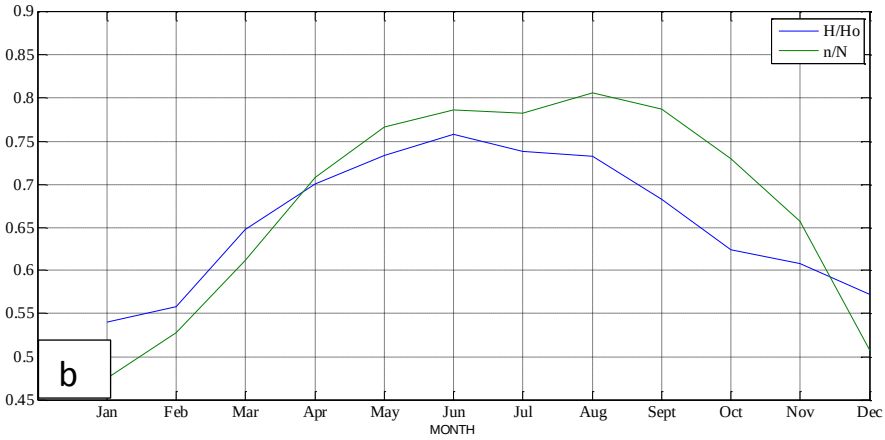
H/Ho
n/N
b
MONTH

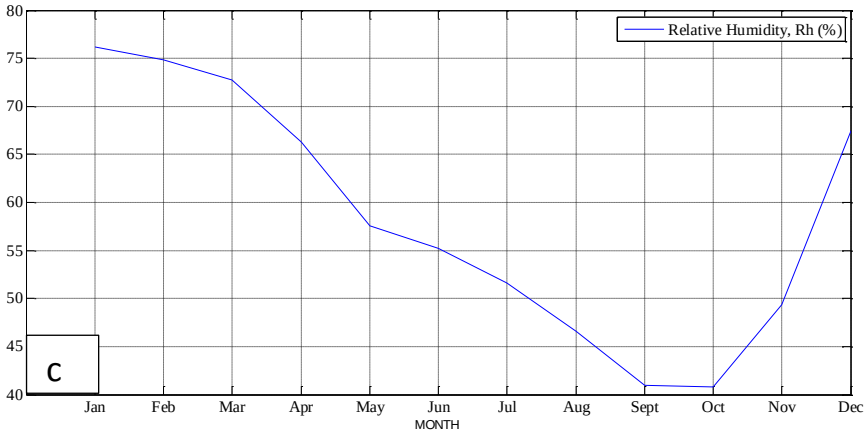
Relative Humidity, Rh (%)
c
MONTH

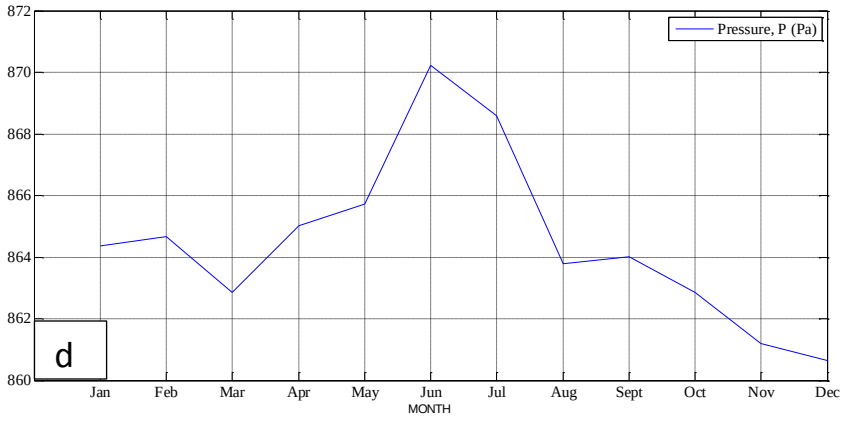

Figure 4.5 Monthly mean daily variations of the considered parameters (a) T_{max}, Cloud Cover C, T_{dpmax} and H_o (b) H/H_o and n/N (c) Relative Humidity, R_h and (d) Pressure at **MFUWE** Station

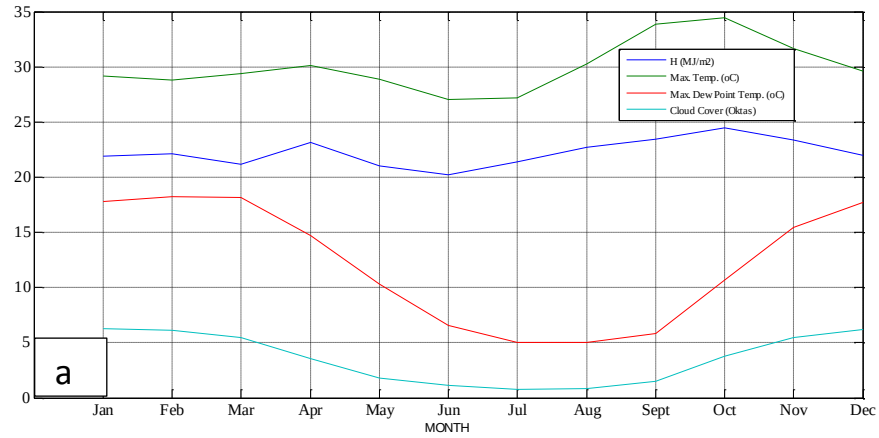

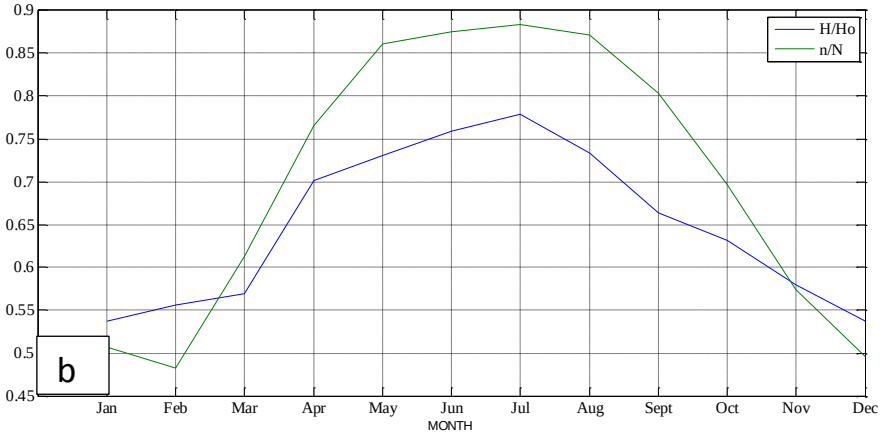

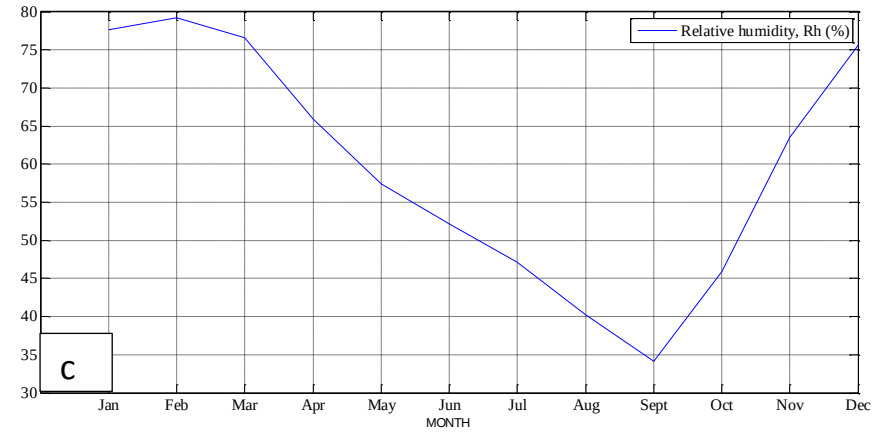

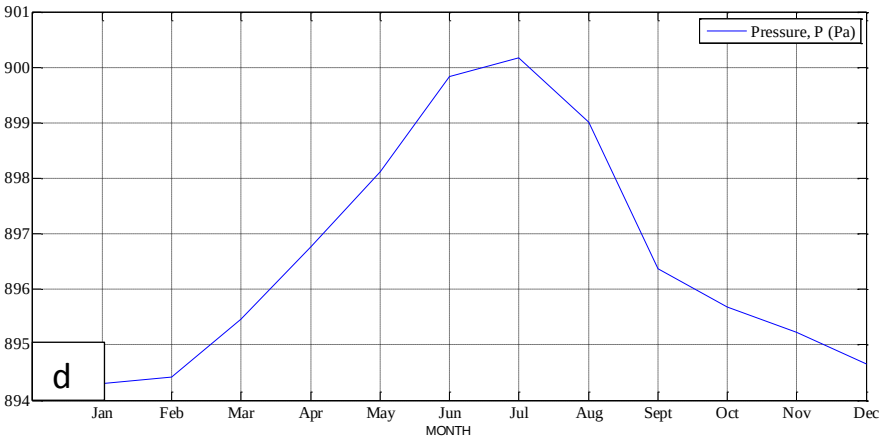

Figure 4.6 Monthly mean daily variations of the considered parameters (a) T_{max}, Cloud Cover C, T_{dpmax} and H_o (b) H/H_o and n/N (c) Relative Humidity, R_h and (d) Pressure at **MONGU** Station

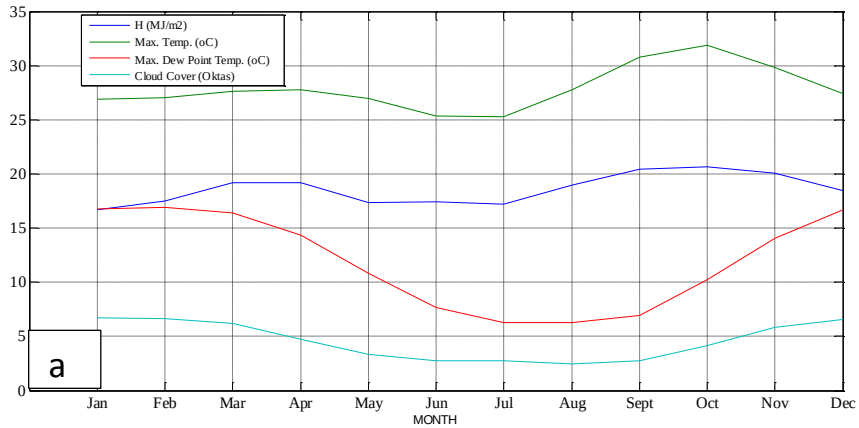

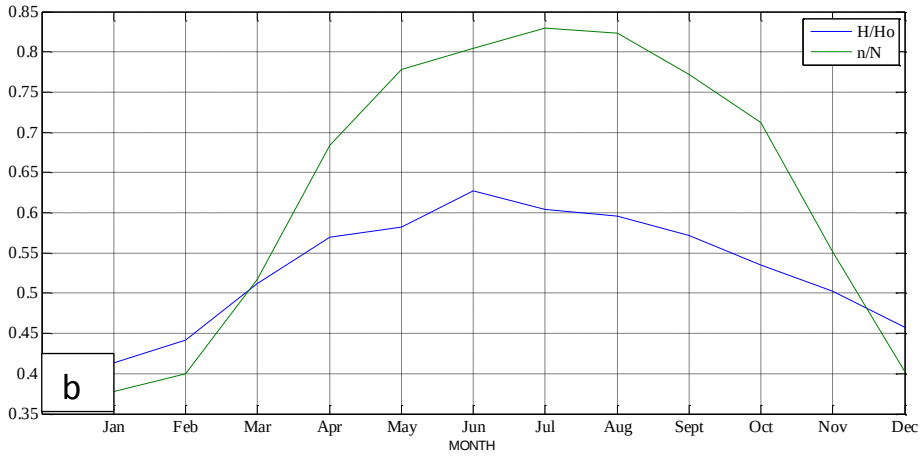

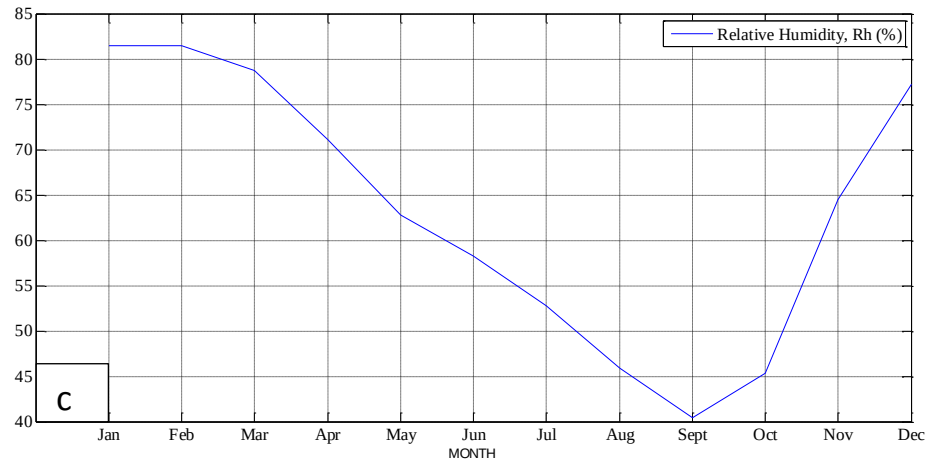

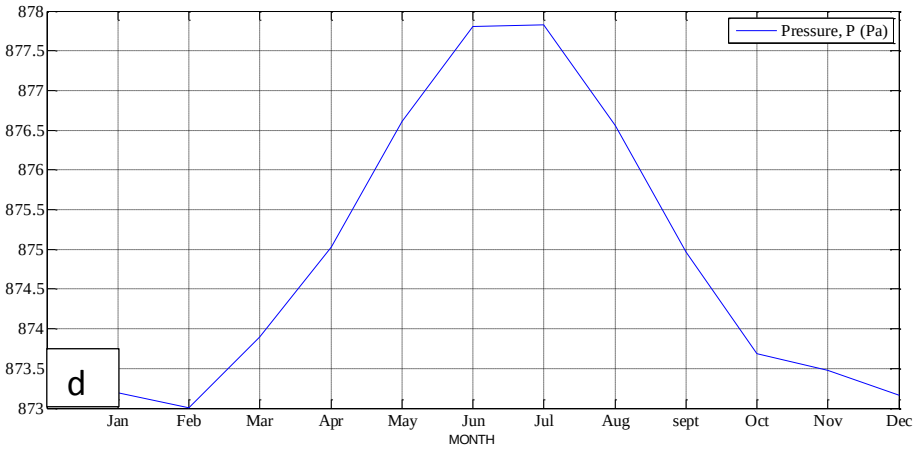

Figure 4.7 Monthly mean daily variations of the considered parameters (a) T_{max}, Cloud Cover C, T_{dpmax} and H_o (b) H/H_o and n/N (c) Relative Humidity, R_h and (d) Pressure at **NDOLA** Station

a) Global Solar Radiation Measurements

The maximum values of global solar radiation at all considered locations appear in October, while the minimum values are in June. The annual average daily values for the global solar radiation on horizontal surface at Kasama is 14.82 MJ/m^2/day, at Livingstone is 17.56 MJ/m^2/day, at Lusaka is 18.76 MJ/m^2/day, at Mansa is 19.39 MJ/m^2/day, at Mfuwe is 22.87 MJ/m^2/day, at Mongu is 22.23 MJ/m^2/day and at Ndola is 18.60 MJ/m^2/day. The values of global solar radiation at Mfuwe and Mongu (south Zambia) are higher than they are in Livingstone, Lusaka and Ndola (middle Zambia), Mansa and Kasama (northern Zambia). This is due to the fact that the daily mean number of hours of the bright sunshine in the south is higher than in the middle and the north, where the values of annual mean of the number of sunshine hours in Mfuwe is 8.1 h and Mongu is 8.37 h, in Livingstone is 9.10 h, in Lusaka is 8.10 h , in Kasama is 7.75 h , in Mansa is 7.64 h and in Ndola 7.59 h.

b) **Maximum Temperature (T_{max})**

The monthly daily mean of maximum temperatures has higher values in October and lower values in July at all locations. The annual mean values of the maximum temperatures are 27.27, 29.96, 26.40, 24.06, 28.17, 32.85, 30.02 and 27.87 ^oC at Kasama, Livingstone, Lusaka, Mansa, Mfuwe, Mongu and Ndola respectively. The values increase as one moves from the north toward south because the solar declination angle at the north is smaller than at the middle and the south of Zambia.

c) **Relative Humidity as a Percentage (R_h)**

The graphs have the same trend where the maximum values were in January/ February and the minimum values were in September. This is because of the rainy season in January and dry season in October. The annual mean values of the relative humidity are 66.58, 55.67, 63.01, 64.84, 58.30, 59.62 and 63.32% at Kasama, Livingstone, Lusaka, Mansa, Mfuwe, Mongu and Ndola respectively.

d) Cloud Cover, (C)

Cloud Cover has maximum values in January and December while the minimum values occur in July for all the selected locations.

e) Maximum Dew Temperature ($T_{dp, max}$)

The monthly variation of maximum dew point temperature have the same trend, where the maximum values for each were in January and December and the minimum values were in July and August.

f) Pressure

The maximum monthly variation values of Pressure were in June and July at all locations, while the minimum values were in January and February.

4.1.2 Comparison between ground measured and satellite derived solar data sets

Table 4.1 shows global solar radiation satellite derived data for selected sites in Zambia, provided by web-based systems and databases, **NASA Surface Meteorology and Solar Energy (SMSE 2012)** compared with ground measured data**.** Figures 4.8 – 4.14 show the plots for the comparisons of ground measured and satellite derived global solar radiation data sets at (a) Kasama (b) Livingstone (c) Lusaka (d) Mansa (e) Mfuwe (f) Mongu and (g) Ndola stations.

Table 4.1 Comparison of ground measured and satellite derived global solar radiations in $MJ/m^2/day$

Months	Towns													
	Kasama		Livingstone		Lusaka		Mansa		Mfuwe		Mongu		Ndola	
	Ground	Satellite	Ground	Satellite	Ground	Satellite	Ground	Satellite	Ground	Satellite	Ground	Satellite	Ground	Satellite
January	13.092	21.384	16.958	19.512	18.328	19.872	16.909	20.556	21.815	20.160	21.921	19.476	16.677	20.268
February	13.159	22.824	17.710	22.212	17.055	22.536	17.356	22.500	22.094	22.140	22.098	22.140	17.497	22.500
March	14.382	23.616	17.236	25.056	17.942	24.768	18.296	24.084	24.255	24.156	21.178	24.480	19.206	24.264
April	15.149	23.508	16.775	27.684	18.905	27.108	19.259	25.020	23.554	25.704	23.149	26.064	19.214	26.172
May	14.684	20.772	15.948	27.432	17.599	25.992	19.717	23.256	21.757	24.120	21.013	25.848	17.366	24.480
June	13.784	17.892	15.480	28.404	16.670	26.100	19.866	21.924	20.922	23.580	20.193	25.272	17.418	23.400
July	13.563	17.100	15.400	26.964	16.973	23.508	20.154	20.196	20.970	21.456	21.378	23.508	17.241	21.348
August	16.039	17.172	19.238	25.308	19.568	23.004	21.547	19.764	23.227	21.204	22.685	22.824	18.952	20.808
September	17.863	18.828	18.929	24.552	20.713	23.004	21.741	21.168	24.374	21.996	23.422	23.004	20.457	21.780
October	17.070	19.944	18.731	22.932	21.754	22.644	20.508	20.700	24.115	21.960	24.437	22.284	20.672	21.456
November	15.274	21.276	19.080	21.132	20.660	21.564	19.707	20.736	24.315	20.664	23.388	20.952	20.060	21.024
December	13.771	20.916	19.243	18.288	18.947	19.044	17.617	19.872	23.064	19.368	21.957	18.792	18.423	19.620

Figures 4.8 – 4.14 show the plots of the ground measured compared with the satellite-derived global solar radiation data sets for Kasama, Livingstone, Lusaka, Mansa, Mongu and Ndola stations.

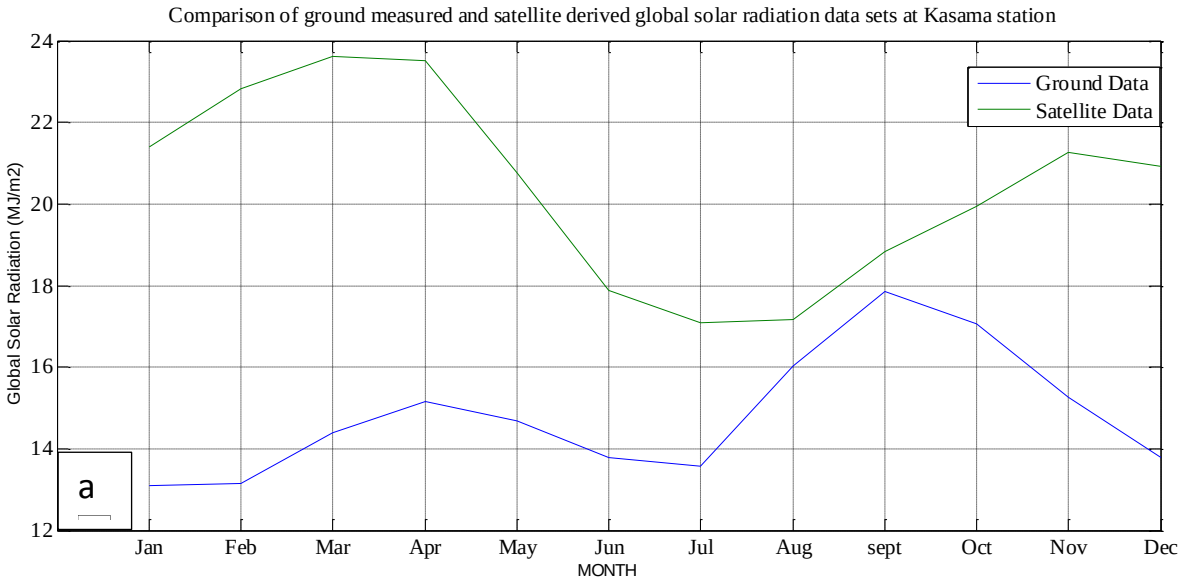

Figure 4.8 Comparisons of ground measured and satellite derived global solar radiation data sets at Kasama

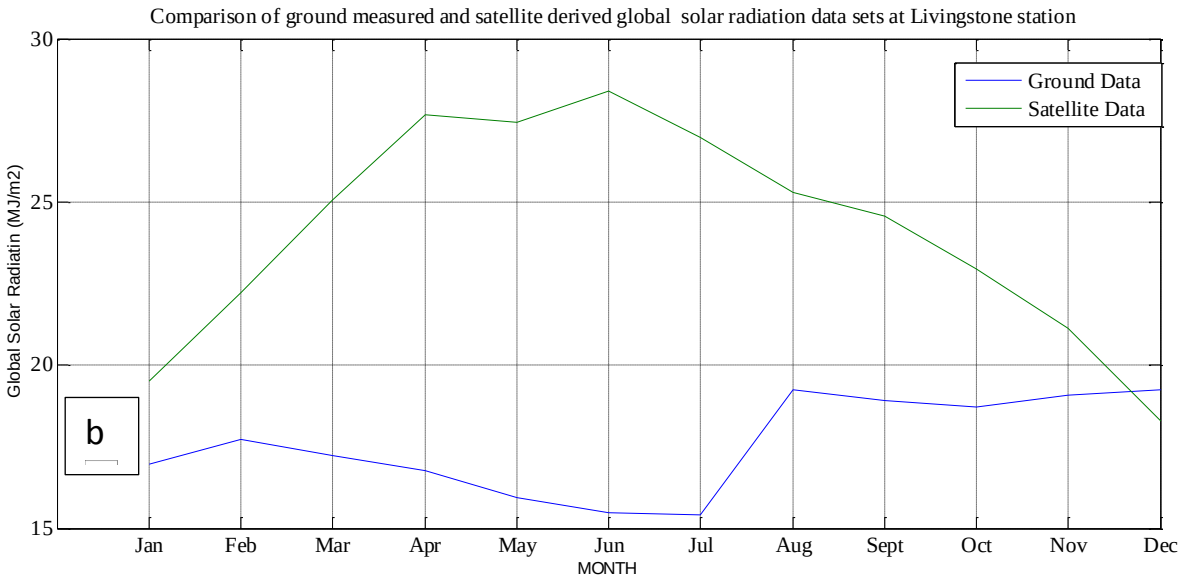

Figure 4.9 Comparisons of ground measured and satellite derived global solar radiation data sets at Livingstone

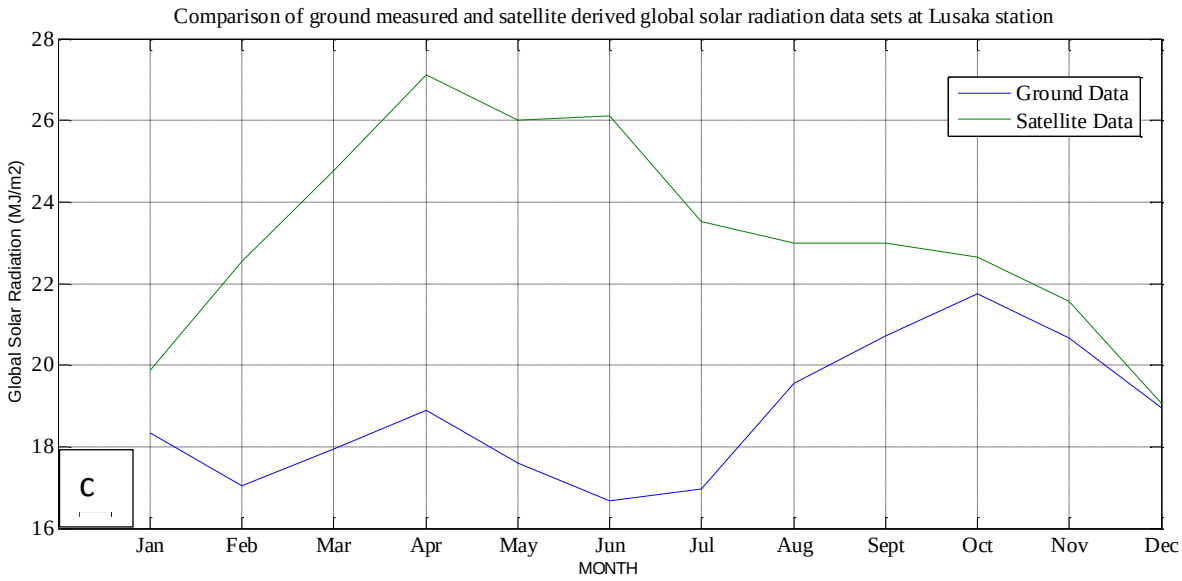

Figure 4.10 Comparisons of ground measured and satellite derived global solar radiation data sets at Lusaka

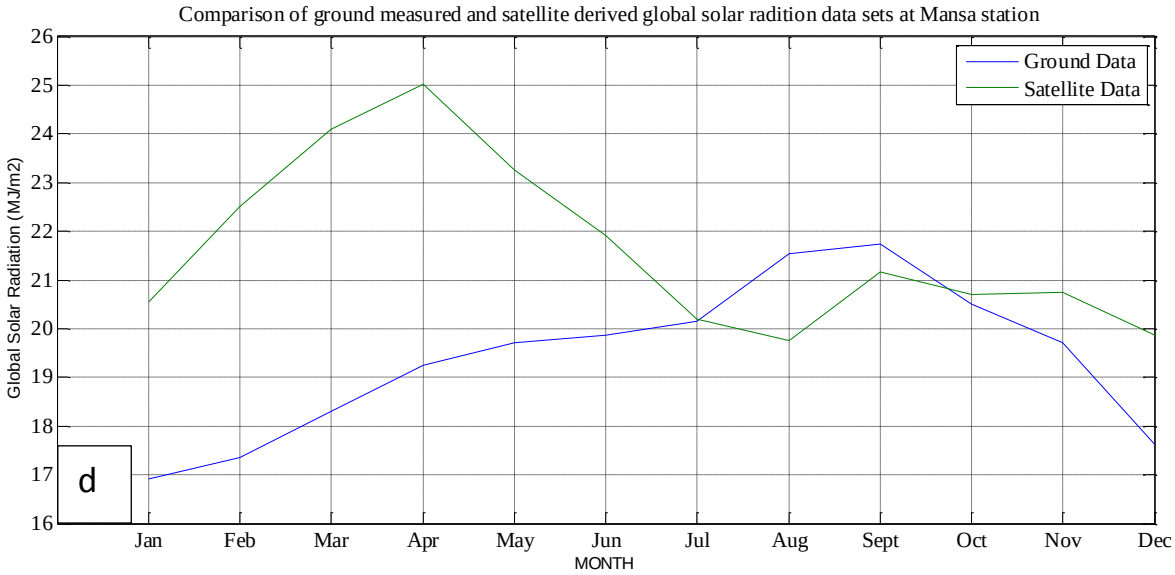

Figure 4.11 Comparisons of ground measured and satellite derived global solar radiation data sets at Mansa

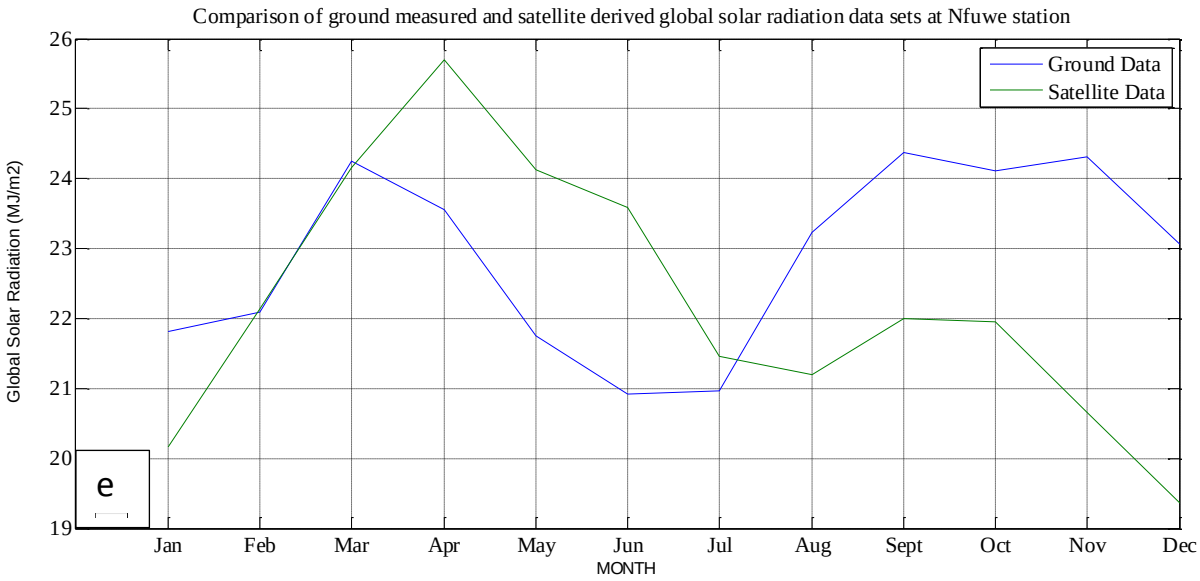

Figure 4.12 Comparisons of ground measured and satellite derived global solar radiation data sets at Mfuwe

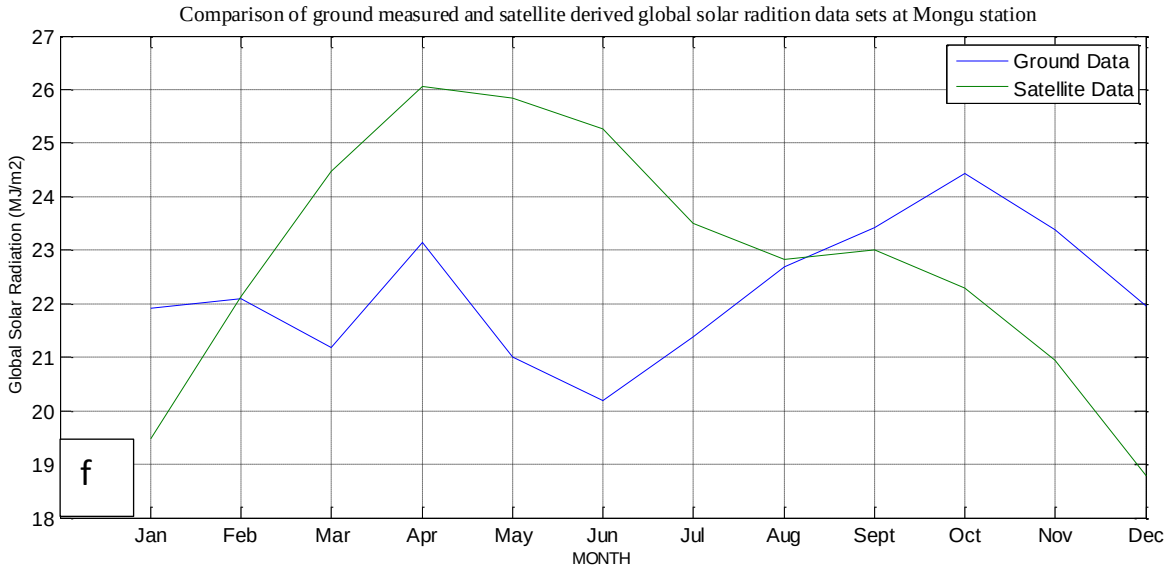

Figure 4.13 comparisons of ground measured and satellite derived global solar radiation data sets at Mongu

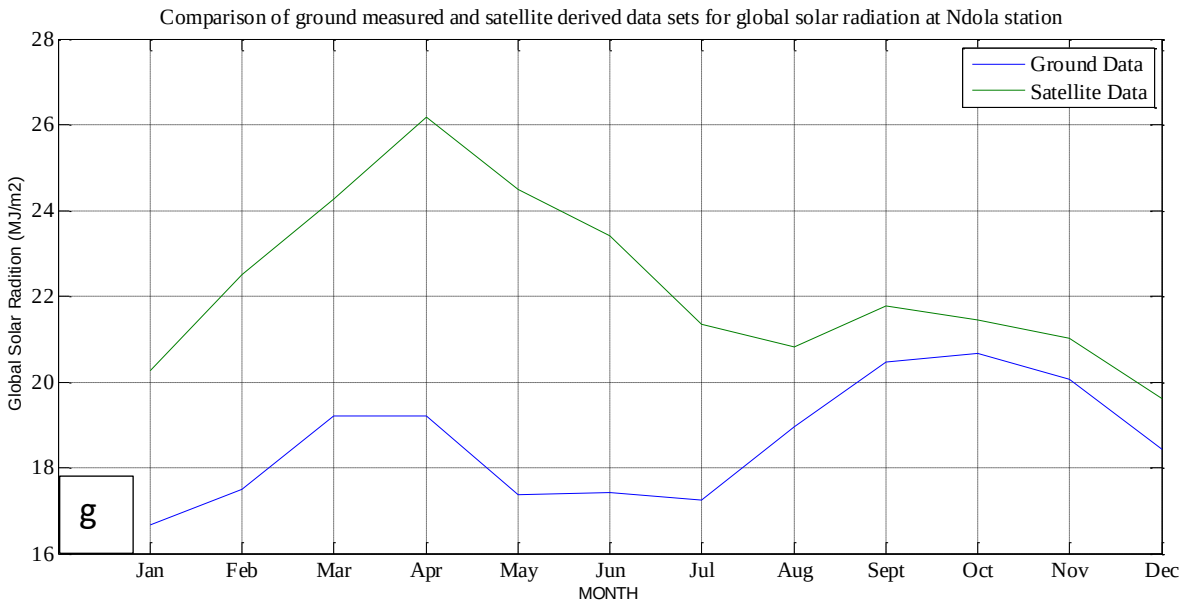

Figure 4.14 Comparisons of ground measured and satellite derived global solar radiation data sets at Ndola

From the plots, the correlation between the satellite-derived database and the ground based data is a very poor for all the locations. In the Figures 4.8- 4.14, the maximum values of global solar radiations derived from satellite imagery occur in April while the ground measured ones are in October. The minimum global solar radiations for satellite derived are between January and December as compared to ground measured ones which occur in May/ June.

The discrepancies could have been as a result of the following:

- The methodology used to develop the satellite model. Only ground-based sites with high quality data should be utilized when trying to develop improved satellite models.
- Testing satellite-derived solar radiation data is not straightforward since satellite images over large areas (100 km^2 in this example once an hour) and ground-based measurements look at only a small portion of the sky and the data are averaged over an hour. Therefore averages and statistics are typically used to compare and contrast these two diverse databases.

4.2 Models for estimating Monthly Mean Global Solar Radiation intensities using Relevant GGAM Parameters for the Selected Locations

In this research, new empirical models were developed which take the form (Eqn. 3.7):

$$H = a + b\sin\delta + cH_o + d\,{}^{n}/_{N} + eR_h + fT_{max} + gT_{dp,max} + hP + iC$$

The measured data of global solar radiation and the meteorological parameters, collected from ZMD and provided in the Compact Disc (CD) at the end of the report was analysed and presented Tables A1 – A8 in Appendix A for all the selected locations in Zambia namely; Kasama, Lusaka, Livingstone, Mansa, Mfuwe, Mongu and Ndola. The data was further processed and analyzed using an advanced computer program Matlab 2011b to obtain the correlation and the regression coefficients *a, b, c, d, e, f, g, h*, and *i* in Eqn. 3.5. The obtained values of correlation coefficients (CC) and the standard errors of estimation (SE) besides the regression coefficients are listed in **Table 4.2.**

Table 4.2 Geographic location of the selected stations and regression and correlation coefficients of estimate for the models (1-7):

Location	Latitude (o) S	Longitude (o) E	*a*	*b*	*c*	*d*	*e*	*f*	*g*	*h*	*i*	CC%	SE
Kasama	10.2117	31.11783	2218.775687	0.59936	0.09446	8.1852039	0.047547	-0.09749	0.35822	-2.5546	-2.5266	0.9752	0.24128
Livingstone	17.8500	25.8667	61.73746035	17.8513	1.65722	-10.444033	-0.58871	-2.24675	1.58705		-2.6337	0.7855	0.68272
Lusaka	15.4167	28.2833	-585.6600048	-11.6302	0.49897	21.791826	0.202466	-0.28998	0.04728	0.65853	-2.3639	0.8735	0.58503
Mansa	11.2000	28.8833	-53.81102774	0.59584	0.49997	0.8099938	0.321402	1.039969	0.04556	0.02287	-3.4939	0.8738	0.55748
Mfuwe	13.2586	31.9364	195.6131526	-3.06813	0.38094	26.886904	0.064175	-0.2344	0.11693	-0.2329	-0.2243	0.8229	0.55037
Mongu	15.2775	23.1319	-1293.999502	0.51954	0.37105	-10.498443	0.358252	1.567532	-0.4234	1.39702	-1.4918	0.529	0.83637
Ndola	12.9667	28.6333	-4134.002409	14.904	1.54283	-15.994826	-0.46305	0.376909	1.66861	4.69168	0.50534	0.7087	0.73601
All Zambia			-86.92549535	0.34393	0.51441	12.127637	0.004943	0.036789	0.14021	0.0917	-0.8268	0.7633	0.59491

From table 4. 2, the formulae of empirical models investigated were written as follows:

1. Kasama Model

   $$H = 2218.7757 + 0.5994\sin\delta + 0.0945H_o + 8.1852\,{}^{n}/_{N} + 0.0475R_h - 0.0975T_{max} + 0.3582T_{dp,max} - 2.5546P - 2.5266C$$ Eqn. 4.1

2. Livingstone Model

   $$H = 61.7375 + 17.8513\sin\delta + 1.6572H_o - 10.4440\,{}^{n}/_{N} - 0.5887R_h - 2.2468T_{max} + 1.5870T_{dp,max} - 2.6337C$$ Eqn. 4.2

3. Lusaka Model

$$H = -585.6600 - 11.6302\ \sin\delta + 0.4990H_o + 21.7918\,{}^{n}/_{N} + 0.2025R_h - 0.2900T_{max} + 0.0473T_{dp,max} + 0.6585P - 2.3639C \quad \text{Eqn. 4.3}$$

4. Mansa Model

$$H = -53.8110 + 0.5958\sin\delta + 0.5000H_o + 0.8100\,{}^{n}/_{N} + 0.3214R_h + 1.0400T_{max} + 0.0456T_{dp,max} + 0.0229P - 3.4939C \quad \text{Eqn. 4.4}$$

5. Mfuwe Model

$$H = 195.6132 - 3.0681\sin\delta + 0.3809H_o + 26.8869\,{}^{n}/_{N} + 0.0642R_h - 0.2344T_{max} + 0.1169T_{dp,max} - 0.2329P - 0.2243C \quad \text{Eqn. 4.5}$$

6. Mongu Model

$$H = -1293.9995 + 0.5195\sin\delta + 0.3711H_o - 10.4984\,{}^{n}/_{N} + 0.3583R_h + 1.5675T_{max} - 0.4234T_{dp,max} + 1.3970P - 1.4918C \quad \text{Eqn. 4.6}$$

7. Ndola Model

$$H = -4134.9924 + 14.9040\sin\delta + 1.5428H_o - 15.9948\,{}^{n}/_{N} - 0.4630R_h + 0.3769T_{max} + 1.6686T_{dp,max} + 4.6917P + 0.5053C \quad \text{Eqn. 4.7}$$

The above models can be used to estimate global solar radiations in areas where climatological conditions are similar with sufficiently high accuracy.

4.3 Model to estimate solar radiation for all Zambia.

Having developed models for Kasama, Livingstone, Lusaka, Mansa, Mfuwe, Mongu and Ndola, The data in the Appendix A in tables 4.3 – 4.9 was combined to obtain data in Table 4.10 for Zambia and then processed in Matlab 2011b in order to determine the regression coefficients for the model to estimate global solar radiation for all locations in Zambia as in table 4.2 to fit in the model below:

$$H = -86.9255 + 0.3439\sin\delta + 0.5144H_o + 12.1276\,{}^{n}/_{N} + 0.0049R_h + 0.0368T_{max} + 0.1402T_{dp,max} + 0.0917P - 0.8268C \quad \text{Eqn. 4.8}$$

4.4. Comparison between ground measured and estimated values of global solar radiation at selected locations

The values of global solar radiation calculated in the models in Eqn. 4.1 – Eqn. 4.7 were compared with the corresponding measured values as given in Table 4.3 and Figures 4.15 – 4.21.

Table 4.3 Comparisons of ground measured and estimated values of global solar radiation at selected locations (MJ/m^2).

Months	Selected Locations													
	Kasama		Livingstone		Lusaka		Mansa		Mfuwe		Mongu		Ndola	
	Measured Mean	Estimated	Measured Mean	Estimated	Measured Mean	Estimated	Measured Mean	Estimated	Measured Mean	Estimated	Measured Mean	Estimated	Measured Mean	Estimated
January	13.092	12.872	16.958	17.038	18.328	18.256	16.909	17.196	21.815	21.965	21.921	21.876	16.677	16.608
February	13.159	13.407	17.710	17.950	17.055	17.267	17.356	17.529	22.094	22.119	22.098	21.987	17.497	17.450
March	14.382	14.355	17.236	17.121	17.942	18.196	18.296	18.257	24.255	24.333	21.178	21.231	19.206	19.318
April	15.149	15.145	16.775	17.060	18.905	18.890	19.259	19.121	23.554	23.612	23.149	23.114	19.214	19.334
May	14.684	14.790	15.948	16.003	17.599	17.566	19.717	19.871	21.757	21.781	21.013	21.200	17.366	17.411
June	13.784	13.724	15.480	15.345	16.670	16.766	19.866	19.945	20.922	20.811	20.193	20.154	17.418	17.519
July	13.563	13.684	15.400	15.541	16.973	17.023	20.154	20.121	20.970	20.826	21.378	21.371	17.241	17.333
August	16.039	16.082	19.238	19.222	19.568	19.423	21.547	21.608	23.227	23.351	22.685	22.878	18.952	18.789
September	17.863	17.829	18.929	19.033	20.713	20.596	21.741	21.701	24.374	24.125	23.422	23.464	20.457	20.466
October	17.070	17.169	18.731	18.879	21.754	21.891	20.508	20.611	24.115	24.239	24.437	24.479	20.672	20.498
November	15.274	15.252	19.080	19.222	20.660	20.641	19.707	19.667	24.315	24.398	23.388	23.412	20.060	20.100
December	13.771	13.966	19.243	19.440	18.947	18.968	17.617	17.662	23.064	23.085	21.957	21.941	18.423	18.500

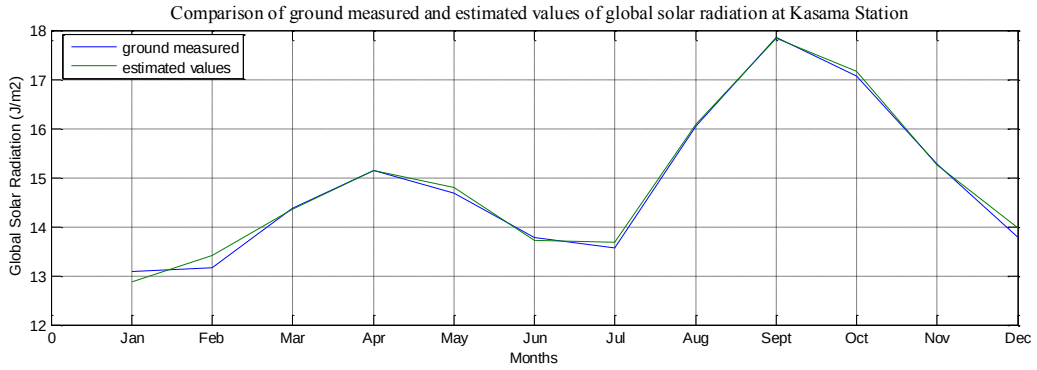

Figure 4.15 Comparisons of ground measured with estimated values of global solar radiation data sets at Kasama.

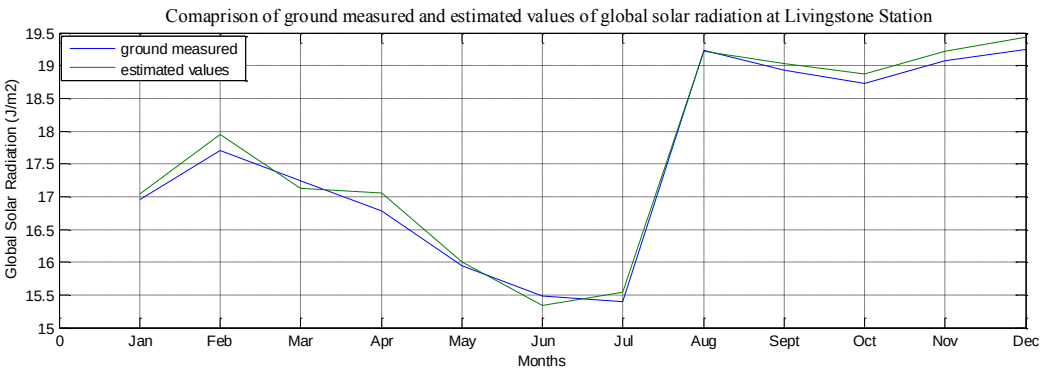

Figure 4.15 Comparisons of ground measured with estimated values of global solar radiation data sets at Livingstone.

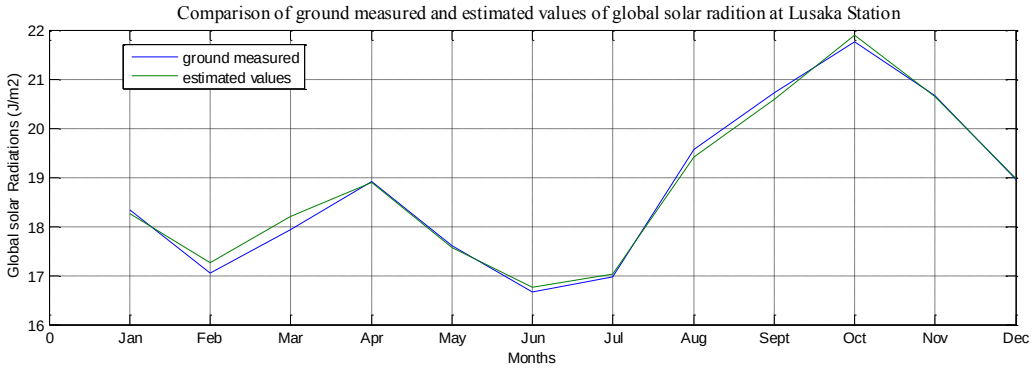

Figure 4.15 Comparisons of ground measured with satellite estimated values of solar radiation data sets at Lusaka.

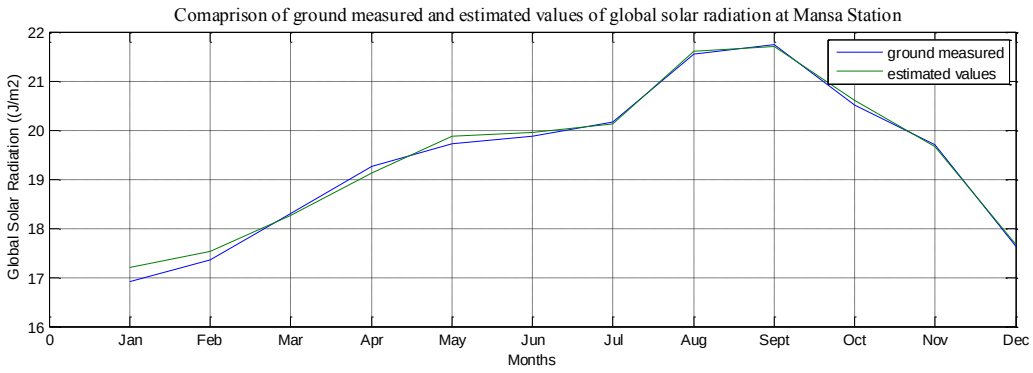

Figure 4.15 Comparisons of ground measured with estimated values of global solar radiation data sets at Mansa.

.

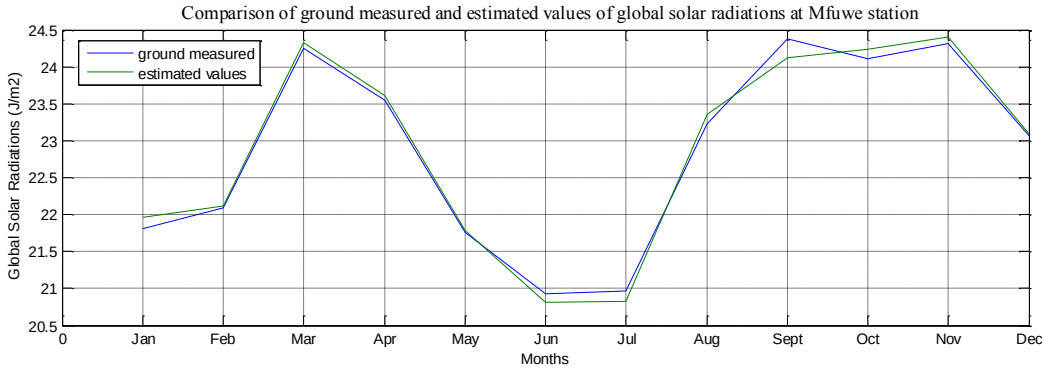

Figure 4.15 Comparisons of ground measured with estimated values of global solar radiation data sets at Mfuwe.

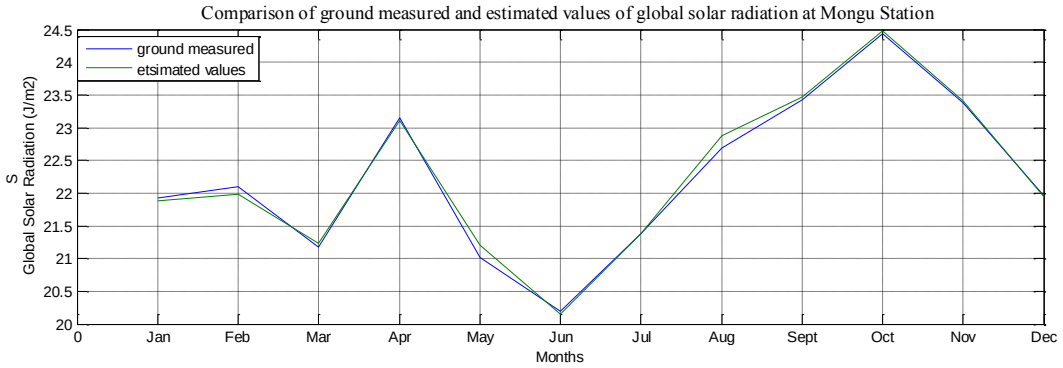

Figure 4.15 Comparisons of ground measured with estimated values of global solar radiation data sets at Mongu

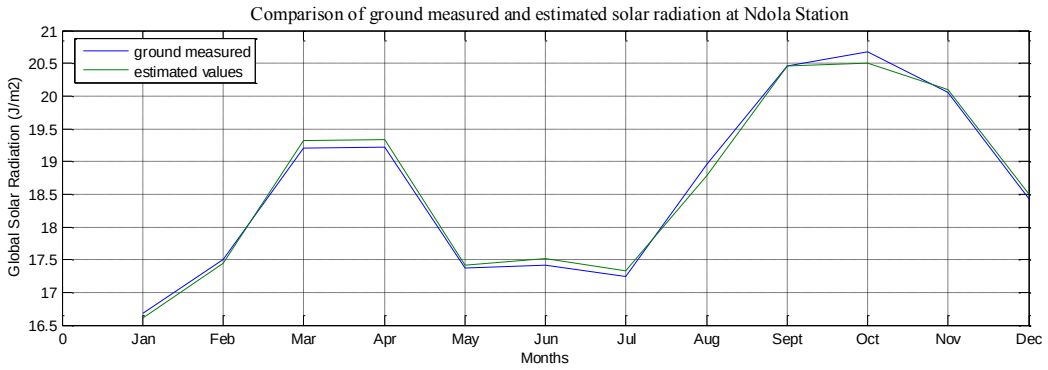

Figure 4.15 Comparisons of ground measured with estimated values of global solar radiation data sets at Ndola.

From the figures 4.15 – 4.21, the deviations between the measured and calculated values are very small. This implies that the models are suitable in calculating the solar radiations at any location in Zambia.

CHAPTER 5 CONCLUSIONS AND RECOMMENDATIONS

5.1 CONCLUSIONS

The current energy situation in Zambia was reviewed and the need for renewable resources was highlighted due to limited nature of fossil fuels. The annual solar radiation (6,600-7,700 MJ/m^2) in Zambia is amongst the highest in the world. With this abundant solar resource, it is expected that the application of solar energy engineering especially; solar water heaters, lighting and refrigeration of medicines at rural health centers will become widespread in the near future. Therefore, the study focused on the estimation of solar radiations for locations in Zambia especially, where this resource is not measured.

The monthly variation of global solar radiation and different meteorological parameters such as sunshine duration, maximum temperature, relative humidity, maximum dew point temperature, cloud cover and pressure are presented and analyzed for seven locations in Zambia. The correlation and regression coefficients for each location and also for all Zambia have been calculated. From the results and considerations, the values of correlation coefficients vary between 97.5% at Kasama and 55.89 % at Mongu and the error did not exceed 0.836. Equations 4.1 – 4.7 are used with high accuracy to estimate the global solar radiation at the selected locations and Equation 4.8 for all Zambia.

5.2 RECOMMENDATIONS

Undoubtedly, a pervasive dearth of solar radiation knowledge exists in Zambia. However, the knowledge of the amount of insolation at various geographic locations is desirable for application in such diverse fields as solar energy utilization, civil engineering, agriculture, forestry, meteorology, environmental assessment, and ecological research.

Therefore, in order to efficiently and effectively utilize the abundant solar energy that the country is endowed with, the following recommendations are made:

- Based on the developed solar model for Zambia in this research, further studies should be carried out to develop a web based program that will input GGAM parameters only in order to get global solar radiation as an output at any particular location in Zambia.

- While no model can fully replace actual measurements to fully assess the potential of a site, the Government of Zambia through the Zambia Meteorological Department (ZMD) should invest in the ‘state of the art’ solar radiation measuring equipment for selected stations with different climatic conditions and continue recording data to generate updated databases for diffuse, direct and global solar radiations.

REFERENCES

André, C., 2007. *World Energy Council,* 2007 Survey of Energy Resources, pp v

Akhlaque, A. M., Firoz, A. and Wasim, M. A., 2009. Estimation of global and diffuse solar radiation for Hyderabad, Sindh, Pakistan. Journal of Basic and Applied Sciences Vol. 5, No. 2, 73-77, 2009 5(2), pp: 73-77.

Applasamy, V., 2011. Methods for Deriving Solar Radiation from Satellite Data in Malaysia. Business, Engineering and Industrial Applications, pp 208 – 213.

Badesu, V. and Joaquin, T. P., 2008. Modelling Solar Radiation at the Earth's Surface, Modelling the Statistical Properties of Solar Radiation and Proposal of a Technique based on Boltzman Statistics, pp 55-91.

Borman, G. L. and Ragland, W., 1998. Combustion Engineering, pp 26

Chow, L. T. and Wong, W. K., 2001. Solar Radiation Model, Applied Energy Volume 69, Issue 3, pp 191–224.

Colorado, U. O., 2003. Laboratory of Atmospheric and Space Physics, http://lasp.cororado.edu/home/missions-projects/quick-facts-sorce/.

El-Sebaii, A. M. and Trabea, A. A., 2005. Estimation of Global Solar Radiation on Horizontal Surfaces over Egypt. Egypt. J. Solids, Vol. 28, No. 1, pp 163- 175.

Fayadh, M. A. A., and Ghazi, Y.M.A., 2010. Estimation of Global Solar Radiation on Horizontal Surfaces over Haditha, Samara, and Beji, Iraq, The Pacific Journal of Science and Technology, Volume11, Number 1, pp 73-82.

Jain, S., and Jain, P. C., 1988. A comparison of Angstrom-type correlations and the estimation of monthly daily global irradiation. Solar Energy, Solar Energy, Volume 40, Issue 2, pp 93-98

Jerome, C. G., 2008. 2020 Global Energy Scenario, http://.www.millennium-project.org/millennium/scenarios/energy-scenarios.html.

Janjai, S. I. M., S. Pattarapanitchai, and J. Laksanaboonsong, 2013. Mapping Global Solar Radiation from Long-Term Satellite Data in the Tropics Using an Improved Mode, International Journal of PhotoenergyVolume 2013 (2013), Article ID 210159.

JICA, 2007. Rural Electrification Master Plan Study in Zambia

Journ´ee, M. C. B., 2010. Geostatistical merging of ground-based and satellite-derived data of surface solar radiation, Advances in Science and Research, Res., 6, 1-5,

Kalsi, S.R., 2003. Satellite based weather forecasting, Satellite Remote Sensing and GIS Applications in Agricultural Meteorology pp. 331-346

Kuster, J.M., 2008. NASA Surface meteorology and Solar Energy: Accuracy, https://eosweb.larc.nasa.gov/sse/

Mapurisa, B. L. S., 2013. Determination of Angstrom Coefficients for Masvingo and Makoholi Stations, Zimbabwe. Journal of Basic & Applied Sciences 9, pp 410-415.

Mathworks, 2007. MATLAB 7 Data Analysis.

Marcel Suri, 2012. Bankable Performance Assessment of PV Projects Using Satellite-based Solar Data. 3rd Annual Conference "PV Power Plants - EU 2012", organised by Solarpraxis, Vienna, Austria, 29-30 March 2012.

Medugu D. W., and Yakubu, D., 2011. Estimation of mean monthly global solar radiation in Yola, Nigeria using Angstrom Model. Advances in Applied Science Research 2(2), pp 414-421.

Nasitwitwi, M. W.,Bailey W.G. and McArthur J.B., 2000. Global Solar radiation in Southern African Savanna Environment.

Nezhad, H., 2009. World Energy scenarios to 2050: Issues and Options.

Paulescu, M., 2013. Weather Modeling and Forecasting of PV Systems Operation, Green Energy and Technology. Springer-Verlag London 2013.

Recipes, 2006. Developing Renewables. http://www.energyrecipes.org/

Rich, P. F. P. M., 2006. Design and Implementation of the Solar Analyst: an ArcView Extension for Modeling Solar Radiation at Landscape Scales. See discussions, stats, and author profiles for this publication at: http://www.researchgate.net/publication/266576778

Safaripour, M.H and Mehrabian M. A. M., 2010. Predicting the direct, diffuse, and global solar radiation on a horizontal surface and comparing with real data. Heat Mass Transfer (2011) 47, pp 1537–1551.

Salima, G., and Chavula M. S. G., 2012. Determining Angstrom Constants for Estimating Solar Radiation in Malawi. International Journal of Geosciences, pp 391-397.

SoDa, 2004. Solar Radiation Data from "http://www.soda -is.com/eng/education/other_solar _data.html.

Sen, Z., 2008. Solar Energy Fundamentals and Modeling Techniques: Atmosphere, Environment, Climate Change and Renewable Energy, pp 102.

Sykes, A. O., 1986. The Inaugural Course Lecture: An Introduction to Regression Analysis. http://www.law.uchicago.edu/files/files/20.Sykes_.Regression.

Tiwari, G. N., 2013. SOLAR ENERGY Fundamentals, Design, Modelling and Applications. pp 28-29.

Trabea, A. A. and El-Sebaii, A. M., 2000. Correlation of global solar radiation with meteorological parameters over Egypt. Renewable Energy 21, pp 297-308.

UNEP, 2005. United National Environment Programme, Global Environment Facility-Renewable Energy Based Electricity Generation for Isolated Mini-Grids, 2005 annual report

Vignola, F. P. H., Richard, P. and Marek, K., 2006. Analysis of satellite derived beam and global solar radiation data. Solar Energy, Volume 81, Issue 6, June 2007, pp 768–772

Weier, J. R. C., 2003. NASA Earth Observatory, http://earthobservatory.nasa.gov/Features/SORCE/

William, B. S. and Geyer, M., 2001. Power from the Sun, pp 48

APPENDIX A

Table A1 Monthly mean daily global solar radiation (H), ratio of bright sunshine (*n/N*), mean daily relative humidity (R_h), mean daily maximum air temperature (T_{max}), mean daily maximum dew point temperature ($T_{dp,\ max}$) sine of the solar declination angle (Sinδ) and Cloud cover (C) at **Kasama**.

Month	H (MJ/m^2/day)	Sinδ	H_o (MJ/m^2/day)	*n/N*	R_h (%)	Tmax (oC)	Tdp (oC)	P (Bars)	C (Oktas)
January	13.0924	-0.3570	39.5787	0.3537	82.4171	26.4802	16.8755	862.2085	6.7698
February	13.1593	-0.2250	39.2963	0.3740	82.7075	26.7323	16.9883	862.1761	6.6892
March	14.3821	-0.0419	39.2963	0.4932	81.3432	26.7804	17.0344	862.4478	6.3892
April	15.1492	0.1633	34.5227	0.6689	76.4335	26.7313	16.0237	863.3129	5.4661
May	14.6844	0.3223	30.9858	0.8129	67.5312	26.2439	12.7500	864.8056	3.8565
June	13.7840	0.3924	29.0811	0.8817	61.5762	24.7561	9.6498	866.0580	2.6863
July	13.5631	0.3616	29.7991	0.8797	57.3941	24.9814	8.0072	866.0497	2.4037
August	16.0388	0.2334	32.7675	0.8557	52.0284	27.0789	8.1018	865.0830	2.2665
September	17.8627	0.0384	36.2338	0.7890	45.3240	29.9342	8.2216	863.5052	2.8184
October	17.0701	-0.1668	38.5369	0.6892	48.1450	31.0225	10.5180	862.4483	4.1988
November	15.2736	-0.3239	39.3247	0.5805	65.7789	29.4439	14.2885	862.2196	5.7559
December	13.7713	-0.3907	39.4148	0.4443	78.2378	27.0625	16.4869	862.2311	6.4373
Annual average	14.8192	0.0005	35.7365	0.6519	66.5764	27.2706	12.9121	863.5455	4.6448

Table A2 Monthly mean daily global solar radiation (H), ratio of bright sunshine (*n/N*), mean daily relative humidity (R_h), mean daily maximum air temperature (T_{max}), mean daily maximum dew point temperature ($T_{dp,\ max}$) sine of the solar declination angle (Sinδ) and Cloud cover (C) at **Livingstone**.

Month	H (MJ/m^2/day)	Sinδ	H_o (MJ/m^2/day)	*n/N*	R_h (%)	Tmax (oC)	Tdp (oC)	P (Bars)	C (Oktas)
January	16.9577	-0.3570	41.3423	0.6703	72.6664	29.9843	16.1480		5.8180
February	17.7097	-0.2250	39.8895	0.5887	74.1179	29.8102	16.4311		5.6787
March	17.2356	-0.0419	36.8305	0.7396	69.3521	30.3803	15.3037		4.8893
April	16.7749	0.1633	32.1224	0.8483	60.2970	30.1636	12.8582		3.4574
May	15.9480	0.3223	27.5559	0.8468	53.8671	28.3166	8.6196		2.5279
June	15.4799	0.3924	25.2443	0.8671	52.3234	25.7714	5.5349		2.4423
July	15.4002	0.3616	26.1542	0.8655	49.6971	25.6240	4.5114		2.5934
August	19.2379	0.2334	29.9246	0.8827	40.9789	28.8370	4.3785		2.1572
September	18.9293	0.0384	34.7427	0.8459	33.8964	32.7906	4.9346		2.4057
October	18.7306	-0.1668	38.6385	0.7845	38.1062	34.5551	8.8252		3.5680
November	19.0800	-0.3239	40.7793	0.6089	53.7718	32.7924	12.8616		5.1593
December	19.2429	-0.3907	41.4890	0.5922	68.9074	30.5003	16.5934		5.8454
Annual average	17.5606	0.0005	34.5594	0.7617	55.6652	29.9605	10.5833		3.8785

Table A3 Monthly mean daily global solar radiation (H), ratio of bright sunshine (*n/N*), mean daily relative humidity (R_h), mean daily maximum air temperature (T_{max}), mean daily maximum dew point temperature ($T_{dp,\ max}$) sine of the solar declination angle (Sinδ) and Cloud cover (C) at **Lusaka**.

Month	H (MJ/m^2/day)	Sinδ	H_o (MJ/m^2/day)	*n/N*	R_h (%)	Tmax (oC)	Tdp (oC)	P (Bars)	C (Oktas)
January	18.3279	-0.3570	40.8589	0.4540	81.9923	26.1371	18.2097	872.6061	6.3511
February	17.0550	-0.2250	39.7771	0.4877	81.7242	26.1668	9.8308	872.8904	6.0875
March	17.9421	-0.0419	37.1890	0.6057	76.4783	26.3820	19.0103	874.1398	5.3912
April	18.9051	0.1633	32.9512	0.7292	66.4750	26.1975	13.7000	875.7143	4.0481
May	17.5994	0.3223	28.7047	0.7727	61.0068	24.7784	8.0751	877.5041	3.2044
June	16.6703	0.3924	26.5186	0.7972	58.7405	22.8875	8.4667	878.0986	3.1730
July	16.9730	0.3616	27.3690	0.7992	54.7712	22.7787	4.0004	878.6381	3.0082
August	19.5680	0.2334	30.8905	0.8319	48.9196	25.6007	0.6100	877.5518	2.7285
September	20.7131	0.0384	35.2862	0.8054	42.9969	29.1069	10.7667	875.9704	2.5622
October	21.7540	-0.1668	38.6807	0.7763	47.3171	30.7702	11.4280	874.5596	3.1571
November	20.6604	-0.3239	40.3935	0.6023	61.0183	29.3744	13.5667	875.0987	4.8564
December	18.9472	-0.3907	40.9066	0.4802	74.6312	26.6095	17.6123	873.0193	6.0253
Annual average	18.7596	0.0005	34.9605	0.6785	63.0060	26.3991	11.2730	875.4826	4.2161

Table A4 Monthly mean daily global solar radiation (H), ratio of bright sunshine (n/N), mean daily relative humidity (Rh), mean daily maximum air temperature (Tmax), mean daily maximum dew point temperature (Tdp, max) sine of the solar declination angle (Sinδ) and Cloud cover (C) at **Mansa**.

Month	H (MJ/m^2/day)	Sinδ	H_o (MJ/m^2/day)	*n/N*	R_h (%)	Tmax (oC)	Tdp (oC)	P (Bars)	C (Oktas)
January	16.9095	-0.3570	39.84724374	0.519101	78.94386	27.34103025	16.02218	876.4627	6.7838
February	17.3559	-0.2250	39.41269233	0.623296	78.49561	27.60388805	15.85786	875.6615	6.7027
March	18.2957	-0.0419	37.65125739	0.691373	78.06209	27.68891843	15.74382	876.1691	6.2764
April	19.2587	0.1633	34.24587397	0.795392	72.66678	27.73371429	14.29821	876.9201	5.1504
May	19.7174	0.3223	30.57174954	0.8574	63.69198	27.37000256	11.74217	878.2646	3.4271
June	19.8657	0.3924	28.61238383	0.725882	60.91267	25.99190476	8.385596	879.7646	2.3938
July	20.1538	0.3616	29.35598741	0.871173	56.876	25.81494834	7.076885	880.6306	2.1480
August	21.5468	0.2334	32.43146151	0.672439	51.6241	28.00068932	7.517845	878.803	2.1867
September	21.7409	0.0384	36.07666659	0.536026	44.36127	31.06078124	8.007779	877.3617	2.8574
October	20.5079	-0.1668	38.58873495	0.499485	50.03604	32.05202704	12.01091	876.0079	4.2686
November	19.7072	-0.3239	39.55290074	0.429042	65.50392	29.83625251	14.76575	876.1	5.6818
December	17.6170	-0.3907	39.72343667	0.477407	76.88984	27.50586642	16.18175	882.5142	6.5193
Annual average	19.3897	0.0005	35.5059	0.6415	64.8387	28.1667	12.3009	877.8883	4.5330

Table A5 Monthly mean daily global solar radiation (H), ratio of bright sunshine (n/N), mean daily relative humidity (Rh), mean daily maximum air temperature (Tmax), mean daily maximum dew point temperature (Tdp, max) sine of the solar declination angle (Sinδ) and Cloud cover (C) at **Mfuwe**.

Month	H (MJ/m^2/day)	Sinδ	H_o (MJ/m^2/day)	*n/N*	R_h (%)	Tmax (oC)	Tdp (oC)	P (Bars)	C (Oktas)
January	21.8151	-0.357	40.36843857	0.475217	76.1932	31.56699693	20.27873	864.3677	6.4565
February	22.0936	-0.225	39.61740968	0.527427	74.84079	31.92722662	20.71492	864.6611	6.2108
March	24.2554	-0.0419	37.45093502	0.611666	72.77255	32.04513726	20.5167	862.8622	5.5712
April	23.5542	0.1633	33.63654733	0.70816	66.25203	31.17409184	17.94719	865.007	4.1744
May	21.7570	0.3223	29.68031467	0.766466	57.60397	31.6376916	14.62882	865.7326	3.4118
June	20.9221	0.3924	27.6088619	0.786581	55.2177	29.30746465	11.70354	870.2365	3.1028
July	20.9702	0.3616	28.40513746	0.782507	51.58065	30.09863616	10.62887	868.5987	3.2920
August	23.2268	0.2334	31.70060746	0.805725	46.54276	32.29479033	11.78224	863.7877	2.9001
September	24.3743	0.0384	35.71489556	0.787541	40.93713	35.87590896	12.60042	864.0131	2.7262
October	24.1151	-0.1668	38.65980107	0.729514	40.83041	37.65459915	14.65755	862.8654	3.4455
November	24.3153	-0.3239	39.99032929	0.657511	49.372	36.95538889	17.0813	861.1956	4.6895
December	23.0638	-0.3907	40.32836137	0.507264	67.44059	33.69641947	20.10578	860.6477	5.9383
Annual average	22.8719	0.0005	35.2635	0.6788	58.2986	32.8529	16.0538	864.4979	4.3266

Table A6 Monthly mean daily global solar radiation (H), ratio of bright sunshine (n/N), mean daily relative humidity (Rh), mean daily maximum air temperature (Tmax), mean daily maximum dew point temperature (Tdp, max) sine of the solar declination angle (Sinδ) and Cloud cover (C) at **Mongu**.

Month	H (MJ/m^2/day)	Sinδ	H_o (MJ/m^2/day)	*n/N*	R_h (%)	Tmax (oC)	Tdp (oC)	P (Bars)	C (Oktas)
January	21.9212	-0.3570	40.82897694	0.507291	77.67388	29.17206409	17.81743	894.3063	6.2522
February	22.0979	-0.2250	39.76851286	0.482913	79.16365	28.77789588	18.22505	894.4247	6.1249
March	21.1782	-0.0419	37.20752246	0.612362	76.55084	29.35729793	18.14935	895.4674	5.4526
April	23.1485	0.1633	32.99679687	0.765708	65.89564	30.12452894	14.74193	896.773	3.5328
May	21.0129	0.3223	28.76885404	0.861095	57.41497	28.8735198	10.34019	898.1212	1.8327
June	20.1926	0.3924	26.59007185	0.874674	52.1372	27.00699306	6.575641	899.8335	1.1065
July	21.3777	0.3616	27.43700575	0.883157	47.16655	27.2111415	5.02325	900.1771	0.8048
August	22.6849	0.2334	30.94409934	0.871195	40.22514	30.25194332	5.018222	899.0168	0.8151
September	23.4219	0.0384	35.315323	0.803606	34.12799	33.83484375	5.808635	896.3717	1.5164
October	24.4373	-0.1668	38.68102993	0.696785	45.9232	34.43689404	10.70706	895.6864	3.7885
November	23.3880	-0.3239	40.36919018	0.573778	63.50553	31.64647479	15.421	895.2274	5.4681
December	21.9574	-0.3907	40.87106582	0.495736	75.7018	29.59306452	17.71789	894.6523	6.1682
Annual average	22.2349	0.0005	34.9815	0.7024	59.6239	30.0239	12.1288	896.6715	3.5719

Table A7 Monthly mean daily global solar radiation (H), ratio of bright sunshine (n/N), mean daily relative humidity (Rh), mean daily maximum air temperature (Tmax), mean daily maximum dew point temperature (Tdp, max) sine of the solar declination angle (Sinδ) and Cloud cover (C) at **Ndola**.

Month	H (MJ/m^2/day)	Sinδ	H_o (MJ/m^2/day)	*n/N*	R_h (%)	Tmax (oC)	Tdp (oC)	P (Bars)	C (Oktas)
January	16.6772	-0.3570	40.2976911	0.377406	81.50323	26.89697245	16.73657	873.1934	6.7239
February	17.4968	-0.2250	39.59148773	0.39937	81.43656	27.01223445	16.9075	873.0079	6.6622
March	19.2064	-0.0419	37.48228776	0.517052	78.74982	27.59279906	16.38902	873.8948	6.1649
April	19.2143	0.1633	33.72560758	0.683948	71.04638	27.80366815	14.3644	875.0291	4.7338
May	17.3662	0.3223	29.80907422	0.778448	62.81717	26.95744079	10.82802	876.6146	3.3570
June	17.4180	0.3924	27.75335551	0.804368	58.22014	25.34477431	7.643313	877.8055	2.7212
July	17.2409	0.3616	28.5422234	0.829056	52.78847	25.28116935	6.243951	877.8257	2.7179
August	18.9517	0.2334	31.80675129	0.823308	45.87167	27.76056638	6.298035	876.5628	2.4424
September	20.4572	0.0384	35.76900942	0.771631	40.46911	30.75337153	6.951721	874.9614	2.7600
October	20.6723	-0.1668	38.65275902	0.712425	45.30827	31.87816916	10.22521	873.6883	4.1376
November	20.0602	-0.3239	39.9314323	0.551921	64.45427	29.79137609	14.03075	873.4718	5.8009
December	18.4231	-0.3907	40.24573574	0.402336	77.18781	27.37641387	16.65697	873.1664	6.5972
Annual average	18.5987	0.0005	35.3006	0.6376	63.3211	27.8707	11.9396	874.9351	4.5683

Table A8 monthly mean daily global solar radiations (H), ratio of bright sunshine (*n/N*), mean daily relative humidity (R_h), mean daily maximum air temperature (T_{max}), and mean daily maximum dew **Zambia**.

Month	H (MJ/m^2/day)	Sinδ	H_o (MJ/m^2/day)	*n/N*	R_h (%)	Tmax (oC)	Tdp (oC)	P (Bars)	C (Oktas)
January	17.95727812	-0.3570	40.85886859	0.479556	78.77	28.22553786	17.44115	873.8574	6.450748
February	18.13834299	-0.2250	39.77711356	0.497621	78.9266	28.29006907	16.42221	873.8036	6.307994
March	18.92792749	-0.0419	37.1890335	0.610138	76.18699	28.6038285	17.44962	874.1635	5.733543
April	19.42926117	0.1633	32.95116809	0.742805	68.43806	28.56118846	14.84767	875.4594	4.366141
May	18.2979093	0.3223	28.70468087	0.813686	60.56189	27.73964939	10.99771	876.8404	3.088208
June	17.76180896	0.3924	26.51859667	0.819628	57.01826	25.86658757	8.279923	878.6328	2.517996
July	17.95412266	0.3616	27.36898535	0.84433	52.89628	25.96999771	6.49885	878.6533	2.423999
August	20.179274	0.2334	30.89051257	0.820413	46.59866	28.54636377	6.243805	876.8008	2.213783
September	21.07134207	0.0384	35.28615143	0.762716	40.30183	31.90808342	8.184485	875.3639	2.520906
October	21.0410315	-0.1668	38.68072392	0.698318	45.09518	33.19563439	11.19598	874.2093	3.794878
November	20.35494875	-0.3239	40.39347017	0.571999	60.48639	31.40573508	14.57365	873.8855	5.344537
December	19.00324808	-0.3907	40.90662193	0.485622	74.14234	28.9062944	17.33644	874.3718	6.218699
Annual average	19.17637459	0.0005083	34.96049389	0.678903	61.61854	28.93491413	12.45596	875.5035	4.248453